The Astrophysical Journal, 997:150 (20pp), 2026 February 1 https://doi.org/10.3847/1538-4357/ae21cd

How Accurately Can Obscured Galaxy Luminosities Be Measured Using Spectral Energy Distribution Fitting of Near- through Far-infrared Observations?

Duncan Farrah[1,2], Kiana Ejercito[3], Andreas Efstathiou[4], David Leisawitz[5], Athena Engholm[6], Irene Shivaei[7], Matteo Bonato[8], David L. Clements[9], Sara Petty[10], Lura. K. Pitchford[11,12], Charalambia Varnava[4], Jose Afonso[13,14], Carlotta Gruppioni[15], Evanthia Hatziminaoglou[16,17,18], Andrew Hoffman[2], Mark Lacy[19], Brenda C. Matthews[20,21], Conor Nixon[22], Chris Pearson[23,24,25], Berke Vow Ricketti[26], Dimitra Rigopoulou[27], Loren Robinson[28], Locke D. Spencer[29], Lingyu Wang[30,31], David B. Sanders[2], and Gerard van Belle[32]

[1] Department of Physics and Astronomy, University of Hawai‘i at Mānoa, 2505 Correa Rd., Honolulu, HI 96822, USA; dfarrah@hawaii.edu
[2] Institute for Astronomy, University of Hawai‘i, 2680 Woodlawn Dr., Honolulu, HI 96822, USA
[3] Department of Physics, University of California, Santa Barbara, Santa Barbara, CA 93106, USA
[4] School of Sciences, European University Cyprus, Diogenes Street, Engomi, 1516 Nicosia, Cyprus
[5] Exoplanets and Stellar Astrophysics Laboratory, NASA Goddard Space Flight Center, Code 667, 8800 Greenbelt Rd., Greenbelt, MD 20771, USA
[6] Department of Astronomy, University of Illinois Urbana-Champaign, Urbana, IL 61801, USA
[7] Centro de Astrobiología (CAB), CSIC-INTA, Carretera de Ajalvir km 4, Torrejón de Ardoz, 28850, Madrid, Spain
[8] INAF – Istituto di Radioastronomia and Italian ALMA Regional Centre, Via Gobetti 101, Bologna, I-40129, Italy
[9] Department of Physics, Imperial College London, London, UK
[10] NorthWest Research Associates, 3380 Mitchell Ln., Boulder, CO 80301, USA
[11] Department of Physics and Astronomy, Texas A&M University, College Station, TX 77843-4242, USA
[12] George & Cynthia Woods Mitchell Institute for Fundamental Physics and Astronomy, Texas A&M University, College Station, TX 77840, USA
[13] Instituto de Astrofísica e Ciências do Espaço, Universidade de Lisboa, OAL, Tapada da Ajuda, PT1349-018 Lisbon, Portugal
[14] Departamento de Física, Faculdade de Ciências, Universidade de Lisboa, Edifício C8, Campo Grande, PT1749-016 Lisbon, Portugal
[15] Istituto Nazionale di Astrofisica – Osservatorio di Astrofisica e Scienza dello Spazio, via Gobetti 93/3, 40129 Bologna, Italy
[16] European Southern Observatory, Karl-Schwarzschild-Str. 2, 85748 Garching bei München, Germany
[17] Instituto de Astrofisica de Canarias (IAC), E-38205 La Laguna, Tenerife, Spain
[18] Universidad de La Laguna, Opto. Astrofisica, E-38206 La Laguna, Tenerife, Spain
[19] National Radio Astronomy Observatory, Charlottesville, VA 22903, USA
[20] Herzberg Astronomy & Astrophysics Research Centre, National Research Council of Canada, 5071 West Saanich Road, Victoria, BC V9E 2E7, Canada
[21] Department of Physics & Astronomy, University of Victoria, 3800 Finnerty Rd, Victoria, BC V8P 5C2, Canada
[22] Planetary Systems Laboratory, NASA Goddard Space Flight Center, Greenbelt, MD 20771, USA
[23] RAL Space, STFC Rutherford Appleton Laboratory, Didcot, OX11 0QX, UK
[24] The Open University, Milton Keynes, MK7 6AA, UK
[25] Oxford Astrophysics, University of Oxford, Keble Rd, Oxford, OX1 3RH, UK
[26] Disruptive Space Technology Centre, RAL Space, STFC-Rutherford Appleton Laboratory, Didcot, OX11 0QX, UK
[27] Department of Physics, University of Oxford, Keble Road, Oxford, OX1 3RH, UK
[28] Department of Astronomy, University of Wisconsin-Madison, 475 N. Charter St., Madison, WI 53706, USA
[29] Institute for Space Imaging Science, Dept. of Physics & Astronomy, University of Lethbridge, AB T1K 3M4, Canada
[30] SRON Netherlands Institute for Space Research, The Netherlands
[31] Kapteyn Astronomical Institute, University of Groningen, The Netherlands
[32] Lowell Observatory, 1400 West Mars Hill Road, Flagstaff, AZ 86001, USA
Received 2025 August 20; revised 2025 November 12; accepted 2025 November 15; published 2026 January 20

Abstract

Infrared-luminous galaxies are important sites of stellar and black hole mass assembly at most redshifts. Their luminosities are often estimated by fitting spectral energy distribution (SED) models to near- to far-infrared data, but the dependence of these estimates on the data used is not well understood. Here, using observations simulated from a well-studied local sample, we compare the effects of wavelength coverage, signal-to-noise ratio, flux calibration, angular resolution, and redshift on the recovery of starburst, active galactic nucleus (AGN), and host luminosities. We show that the most important factors are wavelength coverage that spans the peak in a SED, and dense wavelength sampling. Such observations recover starburst and AGN infrared luminosities with systematic bias below 20%. Starburst luminosities are best recovered with far-infrared observations, while AGN luminosities are best recovered with near- and mid-infrared observations, though the recovery of both are enhanced with near/mid-infrared and far-infrared observations, respectively. Host luminosities are best recovered with near/far-infrared observations, but are usually biased low, by $\gtrsim$20%. The recovery of starburst and AGN luminosity is enhanced by observing at high angular resolution. Starburst-dominated systems show more biased recovery of luminosities than do AGN-dominated systems. As redshift increases, far-infrared observations become more capable and mid-infrared observations less capable at recovering luminosities. Our results highlight the transformative power of a far-infrared instrument with dense wavelength coverage, from tens to hundreds of microns, for studying infrared-luminous galaxies. We tabulate estimates of systematic bias and random error for use with JWST and other observatories.

Unified Astronomy Thesaurus concepts: Far infrared astronomy (529)

1. Introduction

Infrared-luminous galaxies are systems harboring brief (∼tens of Myr), intense phases of star formation and/or supermassive black hole (SMBH) accretion that are at least moderately obscured, leading to high infrared to optical luminosity ratios. These systems are rare in the nearby Universe, but rise rapidly in number density with redshift, such that by $z \sim 1$ they harbor a significant fraction of the comoving star formation rate and SMBH accretion rate densities. They have also been linked to processes such as the merger-driven transformation of disks to spheroids, and active galactic nuclei (AGN)- and/or star formation-based feedback. Reviews of their properties can be found in D. B. Sanders & I. F. Mirabel (1996), A. W. Blain et al. (2002), C. J. Lonsdale et al. (2006), C. M. Casey et al. (2014), and M. Pérez-Torres et al. (2021).

Estimating the starburst, AGN, and host luminosities of infrared-luminous galaxies has been an observational goal since their discovery, and remains so in the era of JWST. The most direct method for estimating these luminosities, and the one that many other methods are calibrated on, is to measure the shape of the ultraviolet through millimeter spectral energy distribution (SEDs), and then use either energy-balance arguments or radiative-transfer modeling to decompose the SED into its starburst, AGN, and host components (E. da Cunha et al. 2008; J. Chevallard & S. Charlot 2016; M. Boquien et al. 2019; C. Varnava & A. Efstathiou 2024). SED fitting is usually performed using photometric or low- to moderate-resolution spectroscopic ($R \lesssim 200$) data, and constrains fits based on the shape of the continuum and broad spectral features such as polycyclic aromatic hydrocarbon (PAH) features. This approach has been used in studies at all redshifts (e.g., D. Farrah et al. 2003, 2016; E. Hatziminaoglou et al. 2008, 2009; C. J. Lonsdale et al. 2015; R. Herrero-Illana et al. 2017; S. Mattila et al. 2018; E. C. Kool et al. 2020; A. Efstathiou et al. 2022; S. Yamada et al. 2023; L. Spinoglio et al. 2024; C. Varnava et al. 2024, 2025).

Understanding how systematic bias and random error (accuracy and precision, respectively) affect the results from SED fitting is essential to their reliable interpretation. Furthermore, planning for future infrared observatories is enhanced by knowing which factors affect the reliability of SED-fitting results (D. Farrah et al. 2019). Both accuracy and precision may depend on which data the SED models are fit to, since SED shapes can be degenerate, especially in the rest-frame near- and mid-infrared for starbursts versus AGN, and the rest-frame near- and far-infrared for starbursts versus their host galaxies. Yet this issue has not been thoroughly investigated. Studies exist that examine how well galaxy properties can be recovered from specific survey designs (e.g., L. Bisigello et al. 2024; M. Bonato et al. 2024), and which compare the results from different SED-fitting codes (L. K. Hunt et al. 2019; C. Pacifici et al. 2023). However, the dependence of recovered luminosities on the data used has been less well-studied (though see C. G. Magris et al. 2015; J. Leja et al. 2019; J. E. Thorne et al. 2023; L. Sommovigo & H. Algera 2025).

In this work, we examine the issues that affect the accuracy and precision of starburst, AGN, and host luminosities recovered via SED fitting of infrared-luminous galaxies. We use a well-studied sample of infrared-luminous galaxies to generate mock observations for fiducial instruments. We then apply a standard SED-fitting approach to those mock observations and compare the derived luminosities to their (assumed) true values. We define our input sample in Section 2. Using their SEDs as the "true" SEDs, we describe the generation of mock observations for fiducial near- to far-infrared instruments that are representative of past, current, and future facilities in Sections 3 and 4. We describe the fits to these mock observations and the recovery of component luminosities in Section 5. We compare the recovered luminosities to their "true" values, and present estimates of the accuracy and precision of luminosity recovery for each instrument, in Section 6. We present our discussion and conclusions in Section 7. Throughout, we adopt the same cosmology as in A. Efstathiou et al. (2022), a spatially flat universe with $H_0 = 70\,\mathrm{km\,s^{-1}\,Mpc^{-1}}$ and $\Omega_\Lambda = 0.7$.

2. Input Sample

As the input sample for our simulations, we adopt the 42 $z < 0.27$ ultraluminous infrared galaxies (ULIRGs) that were observed as part of the HERschel ULIRG Reference Survey (D. Farrah et al. 2013; H. W. W. Spoon et al. 2013; C. Pearson et al. 2016; D. L. Clements et al. 2018). This sample is an ideal input population for our study for three reasons. First, the sample is an almost unbiased set of nearby infrared-luminous galaxies in which the starburst and/or AGN are much brighter than their host galaxies. The selection is detailed in D. Farrah et al. (2013) and comprises nearly all known systems with $L_{\mathrm{IR}} \gtrsim 10^{12} L_\odot$ at $z < 0.27$. The sample thus spans the full range of starburst to AGN dominance, and all four primary optical spectral classes (H II, LINER, Seyfert 2, Seyfert 1). Second, their ultraviolet through millimeter SEDs have been comprehensively modeled using a radiative transfer approach (A. Efstathiou et al. 2022; D. Farrah et al. 2022), giving a library of SEDs, each with a starburst, AGN, and host component, from which to build our "truth" observations. The details are given in A. Efstathiou et al. (2022), but in brief: The starburst (A. Efstathiou & R. Siebenmorgen 2009) is modeled as an exponentially decaying burst in which the free parameters include the initial optical depths of the star-forming clouds, the *e*-folding times of the starburst, and starburst age. The AGN model (A. Efstathiou & M. Rowan-Robinson 1995; A. Efstathiou et al. 1995, 2013) assumes a smooth, tapered disk in which the half-opening and inclination angles of the torus, the ratio of inner to outer radius, and equatorial optical depth are the primary free parameters. The host model assumes a Sérsic profile with $n = 4$, and a mixed distribution of stars and dust. The SEDs have a spectral resolution of $R \simeq 200$ and include PAH features between 3 μm and 13 μm and silicate dust features at 9.7 μm and 18 μm. They do not, however, include mid- or far-infrared fine-structure lines. Finally, a sample size of 42 is a reasonable compromise between having enough objects to assess the range in recovered luminosities and allowing the fitting to complete using moderate computing resources.

We make one simplifying assumption to this sample. A. Efstathiou et al. (2022) find that three objects show evidence for a "polar" dust SED component—dust within the polar regions of the AGN at distances of a few parsecs. Polar dust is thus rare (though see J. Lyu & G. H. Rieke 2022), and

Table 1
The Input Sample to Our Simulations

Name	Redshift	$L_{\rm Tot}^{\rm True}$ $\log_{10}(L_\odot)$	$L_{\rm Sb}^{\rm True}$	$L_{\rm AGN}^{\rm True}$	$L_{\rm H}^{\rm True}$	$W_{6.2}$ (μm)
IRAS 00188–0856	0.128	12.35	12.27	11.45	11.03	0.102
IRAS 00397–1312	0.262	12.97	12.85	12.32	11.19	0.036
IRAS 01003–2238	0.118	12.20	11.88	11.91	10.36	0.055
IRAS 01572+0009 (Mrk 1014)	0.163	12.53	12.39	11.90	11.27	0.064
IRAS 03158+4227	0.134	12.61	12.42	12.14	10.89	0.101
IRAS 03521+0028	0.152	12.38	12.33	11.41	10.05	0.348
IRAS 05189–2524	0.043	12.14	11.89	11.74	10.84	0.043
IRAS 06035–7102	0.079	12.21	12.08	11.32	11.26	0.105
IRAS 06206–6315	0.092	12.17	12.07	11.23	11.08	0.213
IRAS 07598+6508	0.148	12.62	12.34	12.30	9.56	0.011
IRAS 08311–2459	0.100	12.47	12.35	11.75	11.02	0.139
IRAS 08572+3915	0.058	12.17	11.82	11.89	10.27	<0.003
IRAS 09022–3615	0.060	12.23	12.15	11.41	10.56	0.148
IRAS 09320+6134 (UGC 5101)	0.039	12.01	11.93	10.94	10.97	0.250
IRAS 10378+1109	0.136	12.24	11.91	11.92	10.95	0.105
IRAS 10565+2448	0.043	12.05	11.97	10.97	10.97	0.635
IRAS 11095–0238	0.107	12.19	11.77	11.98	10.27	0.054
IRAS 12071–0444	0.128	12.34	12.08	11.93	11.21	0.118
IRAS 12540+5708 (Mrk 231)	0.042	12.54	12.28	12.17	11.02	0.021
IRAS 13120–5453	0.031	12.24	12.18	10.99	11.14	0.528
IRAS 13428+5608 (Mrk 273)	0.037	12.11	12.04	11.24	10.56	0.190
IRAS 13451+1232 (4C 12.50)	0.122	12.28	11.54	12.12	11.38	0.011
IRAS 13536+1836 (Mrk 463)	0.049	11.88	11.36	11.70	10.59	<0.002
IRAS 14348–1447	0.083	12.30	12.12	11.59	11.43	0.249
IRAS 14378–3651	0.068	12.05	11.98	11.15	10.63	0.445
IRAS 15250+3609	0.055	12.02	11.82	11.57	10.40	0.044
IRAS 15327+2340 (Arp 220)	0.018	12.03	11.96	11.06	10.79	0.272
IRAS 15462–0450	0.100	12.10	11.98	11.40	10.61	0.079
IRAS 16090–0139	0.134	12.48	12.43	11.42	10.81	0.093
IRAS 16504+0228 (NGC 6240)	0.024	11.83	11.62	11.09	11.14	0.378
IRAS 17208–0014	0.043	12.35	12.32	10.78	10.83	0.457
IRAS 19254–7245 (SuperAntena)	0.062	12.12	11.85	11.44	11.51	0.074
IRAS 19297–0406	0.086	12.40	12.29	11.53	11.29	0.436
IRAS 20087–0308	0.106	12.43	12.40	10.98	10.99	0.352
IRAS 20100–4156	0.130	12.51	12.42	11.71	10.78	0.139
IRAS 20414–1651	0.087	12.16	12.10	11.16	10.81	0.571
IRAS 20551–4250	0.043	12.01	11.79	11.49	10.93	0.111
IRAS 22491–1808	0.078	12.07	11.87	11.55	10.91	0.403
IRAS 23128–5919	0.045	11.87	11.75	11.12	10.64	0.364
IRAS 23230–6926	0.107	12.16	12.03	11.53	10.36	0.312
IRAS 23253–5415	0.130	12.31	12.05	11.76	11.53	0.288
IRAS 23365+3604	0.064	12.16	12.06	11.42	10.58	0.401

Note. The columns give their IRAS names, redshifts, their assumed "true" total and component rest-frame 1–1000 μm luminosities, and the PAH equivalent width values used to divide the sample into starburst- and AGN-dominated subsamples (Section 2).

less luminous than the starburst or AGN. As such, we exclude the polar dust component from these three objects to give input SEDs of 42 objects whose components are their starbursts, AGN, and host galaxies. The sample and their "true" luminosities are presented in Table 1. Diagnostic plots for the sample can be found in A. Efstathiou et al. (2022) and D. Farrah et al. (2022).

This choice of input sample places two qualifiers on our results. First, they are most relevant to objects whose starburst and/or AGN are at least a factor of 5 times as luminous as their hosts. Our results become less applicable to objects as this ratio declines. Second, our results are most relevant for objects which are drawn at random from a parent population that resembles our input sample (though we consider simulations using subsets of the input population that are starburst or AGN dominated in Section 6.1.3).

3. Simulated Instruments

We consider observations from the following mock near- through far-infrared instruments:

1. *Ns.* A near-infrared spectrograph covering 1.5–5.0 μm. This resembles spectrographs such as SpeX on the NASA Infrared Telescope Facility (J. T. Rayner et al. 2003), NIRS on Gemini (J. H. Elias et al. 2006), IRCS on Subaru (A. T. Tokunaga et al. 1998), the shorter-wavelength modules within the Infrared Spectrograph (IRS) on

Spitzer (J. R. Houck et al. 2004), and NIRSpec on JWST (P. Jakobsen et al. 2022).
2. *Ms.* A mid-infrared spectrograph covering 5–28 μm. This resembles instruments with coverage of both the *N* and *Q* bands, the longer-wavelength modules within the IRS on board Spitzer, and MIRI on board JWST (G. S. Wright et al. 2023). The combination of Ns and Ms resembles the Short-Wavelength Spectrometer instrument on board the Infrared Space Observatory (T. de Graauw et al. 1996).
3. *NMp.* Photometric observations in five bands spanning near- to mid-infrared wavelengths. We adopt band centers and filter widths that resemble commonly used filters on NIRCam (M. J. Rieke et al. 2023) and MIRI on JWST, but the results should be applicable to any choice of filters that populate near- to mid-infrared wavelengths.
4. *Fs.* A far-infrared spectrograph covering 30–300 μm. This instrument is similar to those proposed for concept missions, including the FIRESS (C. M. M. Bradford et al. 2025) on board PRIMA (D. Burgarella et al. 2024; J. Glenn et al. 2025), SAFARI on SPICA (E. Egami et al. 2018), SPIRIT (D. Leisawitz et al. 2007; B. V. Ricketti et al. 2024), and SALTUS (G. Chin et al. 2024; J. Spilker et al. 2024).
5. *Fp.* Photometry in five far-infrared photometric bands, centered at 70, 160, 250, 350, and 500 μm, chosen to match those within the PACS and SPIRE instruments on board Herschel (M. J. Griffin et al. 2010; A. Poglitsch et al. 2010). Fp also resembles future instruments such as Primager on PRIMA (L. Ciesla et al. 2025).

In addition, we consider the following optical and submillimeter instruments:

1. *Opt*. Since optical imaging in at least one band is ubiquitous, we assume that all simulated observations at any redshift include imaging in two optical bands. We select the Sloan Digital Sky Survey (SDSS) *g* and *r* bands, which are almost identical to the *g*- and *r*-band filters on the Vera Rubin Observatory.
2. *Sp.* When considering observations with multiple instruments (Section 6.3), we include a submillimeter instrument that performs photometry at 450 μm and 850 μm. This instrument resembles several ground-based facilities that observe through two low-opacity windows in Earth's atmosphere, including the Atacama Large Millimeter/submillimeter Array, SCUBA2 (W. S. Holland et al. 2013), or AtLAST (T. Mroczkowski et al. 2025). We do not consider observations with Sp on its own as at most redshifts it constrains only the slope of the Rayleigh–Jeans tail of the SED.

The parameters for each instrument are given in Table 2. We assume that all instruments have flat sensitivity curves. This assumption is reasonable, since filters generally have fairly flat sensitivity profiles, and most modern spectrographs, including NIRSpec and MIRI, have sensitivities that vary by less than a factor of 2 across most of their wavelength ranges. The spectral resolutions of many of these instruments are higher than the spectral resolution of the input SEDs, but since our aim is to examine the recovery of infrared luminosities from SED fitting, rather than measuring fine-structure lines, this should not affect our analysis. We note though that if structure in continua at $R \gg 200$ can constrain luminosities, then our analysis will not include this effect.

Table 2
Simulated Instruments, Their Wavelength Ranges, and Fiducial Wavelengths for S/N Calculations (Section 3)

Instrument	λ (μm)	$\lambda_{\rm fid}$ (μm)
Opt[a]	0.45, 0.70	0.45, 0.70
Ns	1.4–4.8	2.0
Ms	5.0–28.0	10.0
NMp	2.2, 4.4, 7.7, 15, 22	2.2, 4.4, 7.7, 15, 22
Fs	30–300	50
Fp	70, 160, 250, 350, 500	70, 160, 250, 350, 500
Sp[b]	450, 850	450, 850

Notes. "Opt" corresponds to the Sloan *g* and *r* filters. For other instrument names: "N," "M," "F," and "S" correspond to near-infrared, mid-infrared, far-infrared, and submillimeter, respectively, and "s" and "p" correspond to spectroscopy and photometry. The NMp filters correspond to JWST F222W, F444W, F777W, F1500W, and F2200W. The Fp filters correspond to Herschel PACS/SPIRE photometry.
[a] Common to all simulations (Section 3).
[b] Only used in multi-instrument simulations (Section 6.3).

4. Observations Generation

Using the input sample SEDs (Section 2) as the "truth," we generate for each instrument (Section 3) mock data to a given signal-to-noise ratio (S/N) at its fiducial wavelength. The S/Ns at other wavelengths are then calculated from the SED of the individual source. We do not consider telescope or astrophysical backgrounds, or confusion noise. This is equivalent to assuming that the source flux densities can be measured to the quoted noise level by a combination of observing parameters and source-extraction methods. This approach affords broad comparisons across wavelength ranges and redshifts as it is agnostic to specific telescopes or survey designs, but restricts how our results should be interpreted, as detailed below.

Telescope and astrophysical backgrounds can limit observations, but the degree depends on the observed wavelength, the brightness of the source, and the telescope. To illustrate, we show in Figure 1 the SED of the ULIRG Mrk 231, together with typical astrophysical backgrounds and telescope backgrounds for three representative facilities. Depending on the parameters of the observation, the source can be orders of magnitude brighter than these backgrounds, or well below them. Furthermore, backgrounds can be substantially reduced by methods such as nodding and chopping (R. Papoular 1983). By not considering these backgrounds, we assume that the combination of telescope properties and observing parameters means that they can be removed, such that their effect is insignificant. This is likely a reasonable assumption in most cases, but may be invalid for very high-redshift sources observed at longer wavelengths with warmer telescopes.

Source confusion arises when there are secondary sources in the instrument beam in addition to the primary source (J. J. Condon 1974). It increases in importance as angular and/or spectral resolution become coarser and exposure time increases (D. W. Hogg 2001; T. T. Takeuchi & T. T. Ishii 2004;

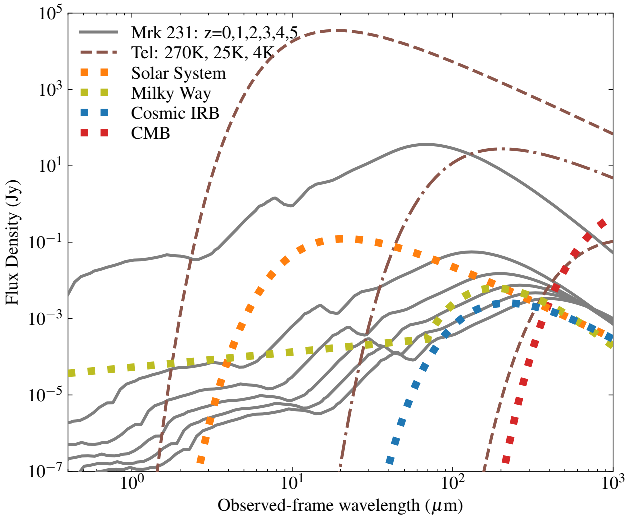

Figure 1. Comparison of telescope and astrophysical backgrounds in a $10'' \times 10''$ aperture, with Mrk 231 at $z = 0, 1, 2, 3, 4, 5$ (Section 4). With $B(T)$ as the Planck function, the telescope backgrounds follow $\epsilon_{\rm tel} B(T_{\rm tel})$ with $\epsilon_{\rm tel} = 0.04$. Zodiacal light is modeled as $2 \times 10^{-7} B(T_{\rm zod})$ with $T_{\rm zod} = 240$ K (C. Leinert et al. 2002). Milky Way emission is modeled via $40((\lambda)/(\lambda_0))^{-\beta} 2 \times 10^{-7} B(T_{\rm ISM})$ (with $T_{\rm ism} = 17.53$ K, $\lambda_0 = 23.05\,\mu$m, and $\beta = 1.55$) for wavelengths longward of $70\,\mu$m, and $5 \times 10^{-23}((\lambda)/(\lambda_0))^{0.4}$ at wavelengths shortward of $70\,\mu$m (D. P. Finkbeiner et al. 1999). For the cosmic infrared background, we adopt $1.6 \times 10^{-5} \left(\frac{\nu}{\nu_0}\right)^{(0.64)} B(T_{\rm IRB})$. The cosmic microwave background (CMB) is modeled as $B(T_{\rm CMB})$, with $T_{\rm CMB} = 2.718$ K (J. C. Mather et al. 1994).

C. Kiss et al. 2005; M. Béthermin et al. 2017; M. Bonato et al. 2024). The confusion limit used to be a straightforward bound on how deeply observations could usefully be performed, as it depended primarily on observed wavelength and telescope aperture, and temperature. This has changed in the last decade. Modern approaches combine advanced statistical methods with prior information including redshift, luminosity, position, angular extent, and SED shape. This allows flux densities to be measured to well below the classical confusion limit (P. D. Hurley et al. 2017; W. J. Pearson et al. 2017, 2018; J. R. Weaver et al. 2023; J. M. Béthermin et al. 2024; J. M. S. Donnellan et al. 2024; L. Wang et al. 2024). Exactly how far below, however, depends on the instrument, the observations, and the source under study. The real-world equivalents of the instruments in our study vary substantially in angular resolution and sensitivity, even for the same observed wavelengths. Accounting for source confusion in our study, in a way relevant to modern analysis methods, would involve simulating a map of each observation at each wavelength with an assumed angular resolution, applying modern source-extraction methods to the ensemble of observations, and then fitting the resulting SEDs. Such an approach is beyond the scope of this work and would render the comparisons across wide wavelength ranges impractical. In not accounting for source confusion, we assume that the instrument, observation, and source properties are such that the observations can be made to the assumed S/N. This approach means our results cannot be directly used to determine the effectiveness of a survey to a fixed flux density limit—the role of source confusion must first be independently estimated to see if observations of a given S/N can be extracted. For this reason, we do not present the luminosity limits as a function of redshift for our results.

5. Parameter Recovery

We fit the simulated observations with the SMART SED-fitting code (C. Varnava & A. Efstathiou 2024). SMART is an updated version of the code used in A. Efstathiou et al. (2022), and uses the same SED libraries. Moreover, C. Varnava et al. (2024) compared key physical quantities derived by SMART with those in A. Efstathiou et al. (2022), and found very good agreement between the estimates. Thus, our results should reflect the degree to which different instruments can recover starburst, AGN, and host properties, rather than differences in model libraries. We restrict our analysis to the CYGNUS AGN model set, with its assumed smooth, tapered disk geometry, since these were used to produce the "true" observations. This means our results do not include error terms for not knowing the true AGN obscurer geometry. These uncertainties may be significant (e.g., F. Gao et al. 2021). We defer an analysis of this issue to a dedicated future work. An example "true" SED, simulated data, and the recovered SED fit to these simulated data are shown in Figure 2.

To assess the quality of the recovery, we compare the following "observed" luminosities to their "true" values:

1. $L_{\rm Tot}$. The total rest-frame 1–1000 μm luminosity of the system.
2. $L_{\rm Sb}$. The rest-frame 1–1000 μm luminosity of the starburst.
3. $L_{\rm AGN}$. The rest-frame 1–1000 μm luminosity of the AGN. This measure of AGN luminosity does not include a correction for anisotropic emission. Recovering the anisotropy-corrected AGN luminosity requires the observations to constrain the geometry of the AGN obscurer. We do not consider this here, but defer it to a future work.
4. $L_{\rm H}$. The rest-frame 1–1000 μm luminosity of the host galaxy.

The other parameters for each model are allowed to vary in the fits, using the same ranges as in A. Efstathiou et al. (2022), but we focus here on how well total and component infrared luminosities can be recovered.

6. Results

6.1. Nearby Universe

We first examine the ability of observations with any one of Ns, NMp, Ms, Fs, and Fp (plus Opt in all cases) to recover total infrared luminosities in the nearby Universe ($z \sim 0.1$). We parameterize this recovery as the ratio of the observed to true luminosity:

$$\alpha = \frac{L^{\rm Observed}}{L^{\rm True}}. \quad (1)$$

We assume that each observation is detected at an S/N of 10σ at its fiducial wavelength. The results are shown in Figure 3 and Table A1. The Fs instrument gives the best recovery, constraining $L_{\rm Tot}$ to within 10% and with little systematic bias. In contrast, the recovery of $L_{\rm Tot}$ with Fp is biased high by about 50%, and low by about 50% with NMp or Ms, on average, with a random uncertainty of ∼30%–40%. With Ns the recovery of $L_{\rm Tot}$ is biased low by about 70%. For $L_{\rm Sb}$, Fs and Fp overestimate by 25% and 50%, on average, Ms and NMp underestimate by 50% and 70%, and Ns gives no useful

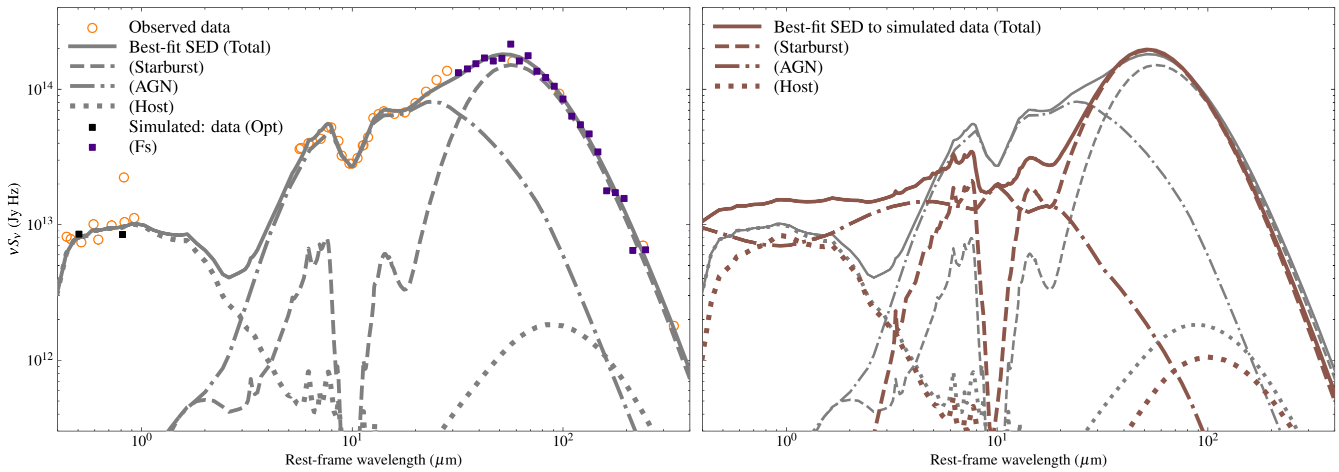

Figure 2. An example of an input SED, simulated data, and recovered fit (Section 5). The left panel shows the original observed data and best-fit SED for Mrk 231 (Figure A7 in A. Efstathiou et al. 2022). Also shown are the simulated Opt and Fs data (Table 2) from this best-fit "truth" SED. The right panel repeats the "truth" SED from the left panel, along with the SED obtained from fitting to the simulated Opt and Fs data. In this case the recovered starburst SED is well matched to the "truth" starburst SED, but the AGN and host components diverge significantly (Section 6.1).

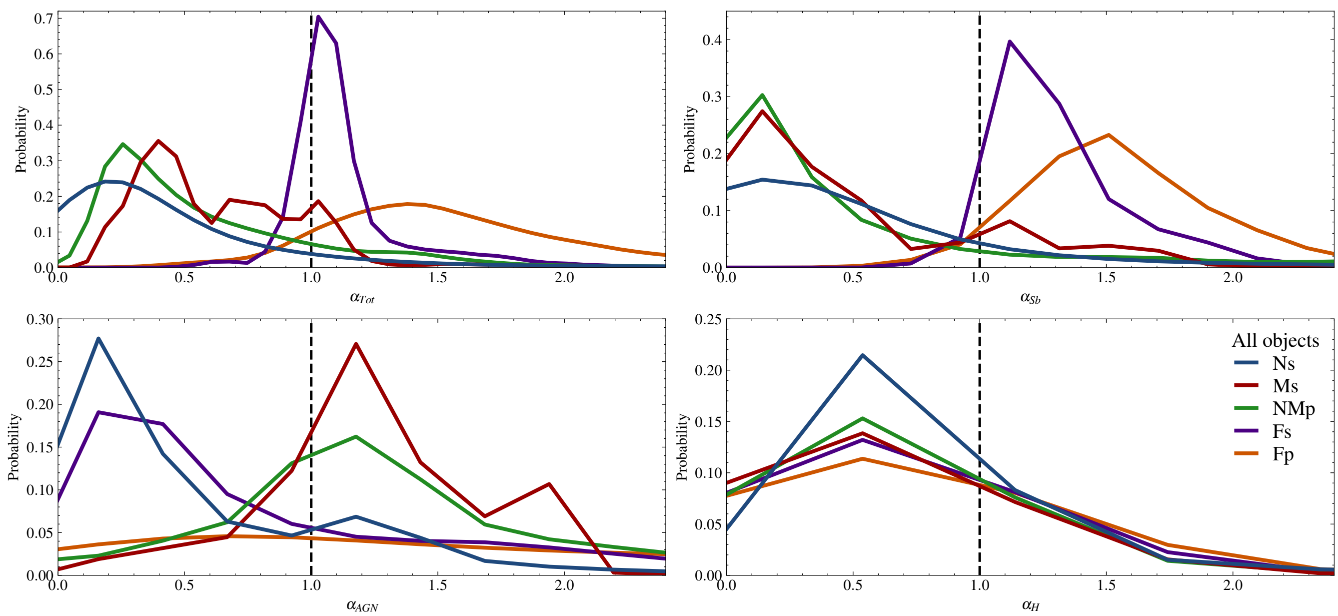

Figure 3. The fractional probability of recovering an observed-to-true luminosity ratio, α (Equation (1)) at $z \sim 0.1$, using observations with the Ns, Ms, NMp, Fs, and Fp instruments individually (Section 6.1). The top-left panel shows the recovery of total infrared luminosity ($L_{\rm Tot}$), the top-right panel shows the recovery of starburst luminosity ($L_{\rm Sb}$), the bottom-left panel shows the recovery of AGN luminosity ($L_{\rm AGN}$), and the bottom-right panel shows the recovery of host-galaxy luminosity ($L_{\rm H}$).

constraints. For $L_{\rm AGN}$, Ms and NMp overestimate by 20%–30%, Fs and Ns underestimate by about 30%, and Fp gives no useful constraints. For $L_{\rm H}$, Ns gives the most accurate recovery, followed by Fs, Fp, NMp, and Ms. All observations systematically underestimate $L_{\rm H}$ by at least 20%, however.

6.1.1. Effect of Signal-to-Noise Ratio

We next explore the effect of varying the S/N of the simulated observations over the range 2–20 (Figure 4). Increasing the S/N from 10 to 20 has no significant impact. Reducing the S/N much below 10, however, does. For all instruments, there is noticeable degradation in the recovery of total, starburst, AGN, and host luminosity by $S/N \simeq 6$, and substantial degradation by $S/N \simeq 4$. Reducing the S/N impacts precision (random error) more than accuracy (systematic bias). Since we do not want our subsequent results to be dominated by S/N effects, we fix $S/N = 10$ for all simulations in the nearby Universe.

6.1.2. Effect of Flux Calibration

Another potential issue is an error in the flux calibration of the instrument. To investigate this, we explore the impact on luminosity recovery of a uniform flux calibration error of between -20% and 20% over the wavelength range of each instrument (Figure 5). For $L_{\rm Tot}$, fitting a linear model between the flux calibration error and the bias in luminosity recovery

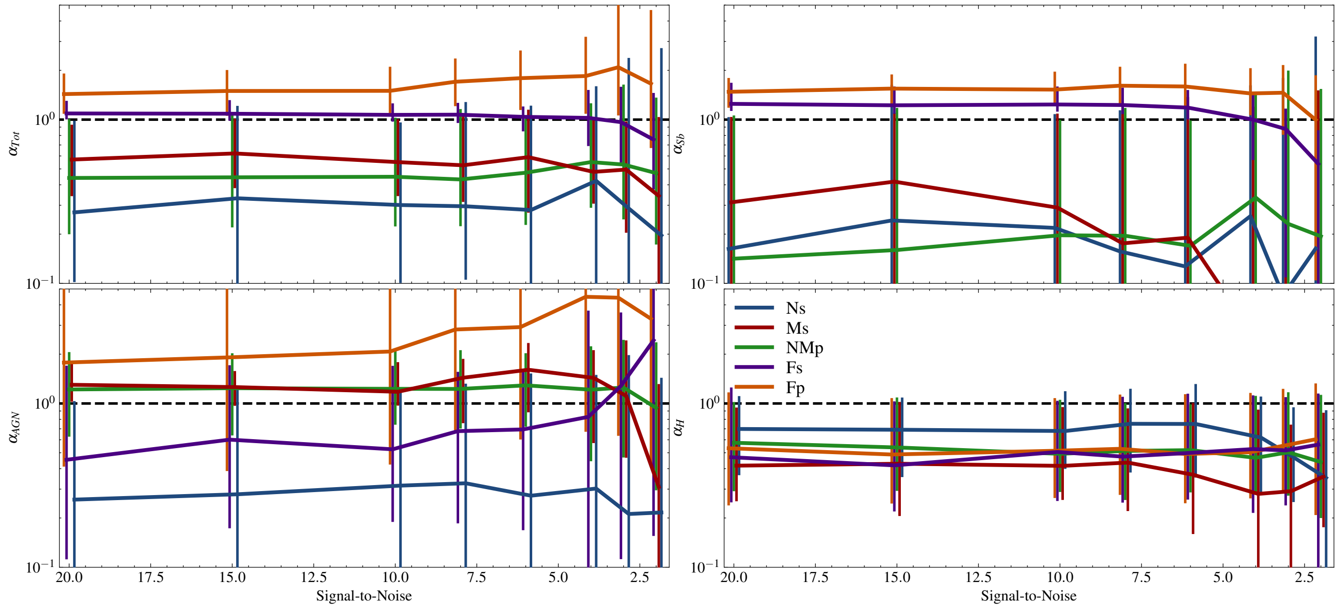

Figure 4. The effect of varying the S/N of the simulated observations on the recovery of total, starburst, AGN, and host luminosity (Section 6.1.1). The lines have been slightly offset in the x-axis for clarity.

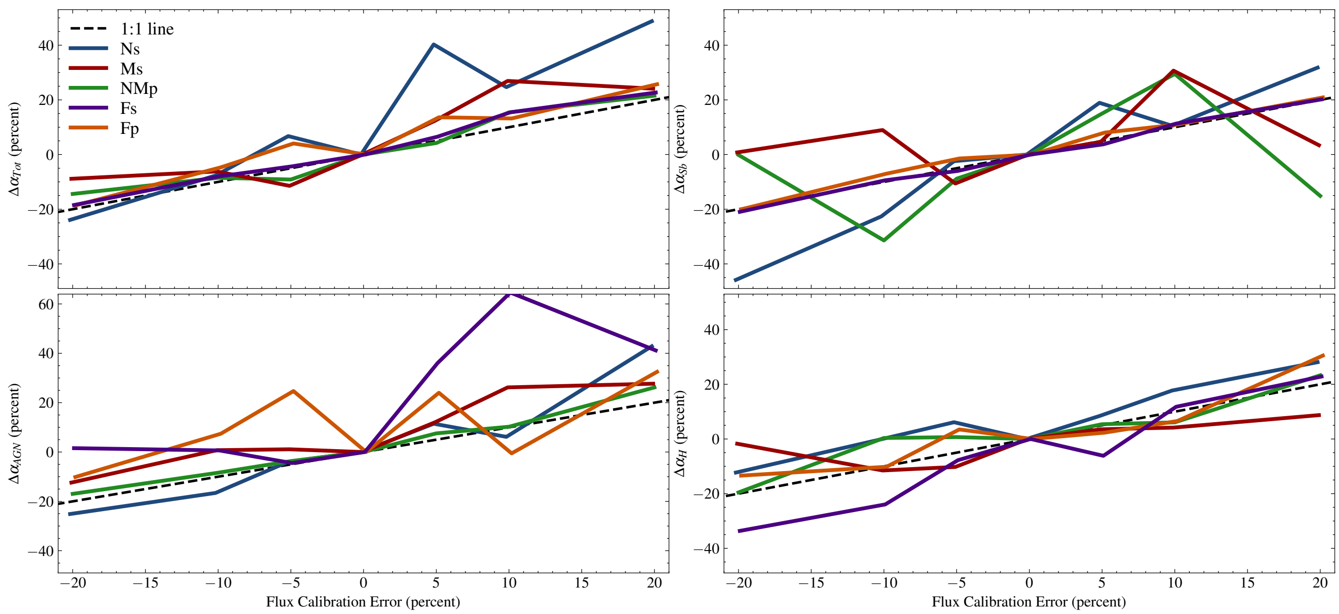

Figure 5. The effect of a flux calibration error on the recovery of total, starburst, AGN, and host luminosity (Section 6.1.2). The lines have been slightly offset in the x-axis for clarity. Error bars have also been omitted for clarity but are comparable in size to those for the S/N = 10 observations in Figure 4.

yields a slope consistent with unity to within 1σ for Ms, NMp, Fs, and Fp, and to within 2σ for Ns. For $L_{\rm Sb}$, the slopes are consistent with unity to within 1σ for Fs and Fp, but show tension with a unity slope at the 2σ–2.5σ level for Ns, Ms, and NMp. For $L_{\rm AGN}$, the slopes are consistent with unity to within 1σ for all instruments except Ns, which is consistent at $\sim 2\sigma$. For $L_{\rm H}$, the slopes are consistent with unity to within 2σ for all instruments except Ms, which is inconsistent with unity at the $\sim 3.5\sigma$ level. These results may suggest the presence of a subtle effect, in which a flux calibration error in a given instrument more strongly impacts the recovery of SED luminosities that are faint in its wavelength range than those that are bright. However, a study with a larger sample would be required to confirm this.

6.1.3. Effect of Starburst versus AGN Dominance

The initial selection of an object may predispose it toward starburst or AGN dominance. Simulations with an input population that spans the full range of starburst to AGN dominance may not be applicable in these cases. Accordingly, we divide our input sample into two subsamples, one with 6.2 μm PAH equivalent widths (EWs) of $W_{6.2} > 0.14$ μm and one with $W_{6.2} < 0.14$ μm. We adopt this criterion as PAH EW is commonly used to select for starburst dominance (V. Desai et al. 2007; J. Bernard-Salas et al. 2009; T. Takagi et al. 2010; Y.-W. Lin et al. 2024), and because this boundary closely divides the sample into systems where more (less) than half of $L_{\rm Tot}$ arises from star formation. This does however mean that the results from each simulation are based on only 21 objects.

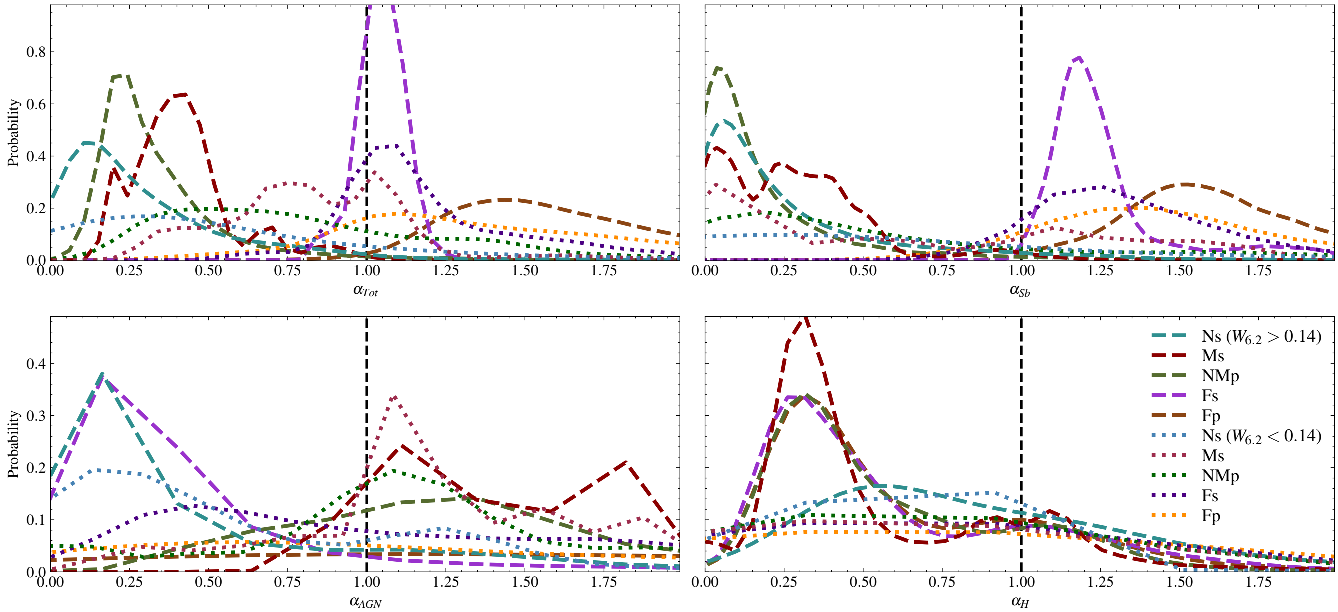

Figure 6. As Figure 3 but using two subsets of the full input population, one with 6.2 μm PAH EWs greater than 0.14 μm (dashed) and one with 6.2 μm PAH EWs less than 0.14 μm (dotted). Axis ranges have been modified to aid comparison (Section 6.1.3).

This should still be sufficient to estimate the recovery of luminosities, but we note this as a caveat to our analysis.

The results are shown in Figure 6 and Table A1. For the $W_{6.2} > 0.14\,\mu$m simulations, the recovery of $L_{\rm Tot}$ and $L_{\rm Sb}$ is biased toward lower values using Ns, Ms, or NMp, but is effectively unchanged for Fs and Fp. For $L_{\rm AGN}$, Ns and Fs become more biased to lower values, while Ms and NMp are unchanged. The recovery of $L_{\rm H}$ is unchanged for any instrument. For the $W_{6.2} < 0.14\,\mu$m simulations, the results are different. For $L_{\rm Tot}$ and $L_{\rm Sb}$, the Ns, Ms, and NMp instruments all give less biased recovery, while the recovery using Fs and Fp is barely changed. For $L_{\rm AGN}$, the recovery with Ns and Fs is slightly less biased, but unchanged with Ms, NMp, or Fp. The recovery of $L_{\rm H}$ is not affected using any instrument.

6.1.4. Effect of Angular Resolution

We here examine the effect on luminosity recovery of observing at finer angular resolution. We consider the scenario where finer angular resolution allows a component SED to contribute more of the emission in an aperture. We focus on the recovery of $L_{\rm Sb}$ and $L_{\rm AGN}$ under the assumption that the host is much larger than the starburst or AGN. We adopt a simple model in which each galaxy has a host of diameter 10 kpc, a starburst of diameter 1 kpc, and an AGN of diameter 0.1 kpc. We assume the light from each component is uniformly distributed over these regions. For ease of comparison with the other results in Section 6, we keep each galaxy at its redshift in Table 1, though moving them all to a common redshift of $z = 0.1$ has an insignificant effect on the results that follow. Then, for $L_{\rm Sb}$, we consider an angular resolution of $1''$, centered on a starburst+host region (finer angular resolutions start to resolve the starburst). For $L_{\rm AGN}$, we consider angular resolutions of $1''$ and $0\overset{''}{.}1$, centered on a starburst+AGN+host region.

The results are shown in Figure 7 and Table A1. For $L_{\rm Sb}$, the $1''$ resolution reduces systematic bias for all instruments. The effect is most marked for the spectrometers, especially for Ms, for which the systematic bias becomes insignificant. The high-PAH EW simulations predict generally larger systematic biases, and the low-PAH EW simulations predict smaller systematic biases. For $L_{\rm AGN}$, the recovery with Ns is only marginally improved by observing at $1\overset{''}{.}0$ or $0\overset{''}{.}1$ resolution. In contrast, with Ms and NMp the recovery is noticeably improved at $1''$ resolution, and improved further at $0\overset{''}{.}1$ resolution. With Fs, there is slight improvement at $1''$ resolution and significant improvement at $0\overset{''}{.}1$ resolution. With Fp, the improvement is marginal. We again see a tendency for the high-PAH EW simulations to show more biased recovery, and the low-PAH EW simulations to show less biased recovery, though the effect is small at $0\overset{''}{.}1$ resolution. An important corollary is that, since we are not including source confusion, these results are lower bounds on the improvement that finer angular resolution provides.

6.2. High-redshift Universe

We here examine luminosity recovery using single-instrument observations over $0 < z < 5$. For these simulations, we assume 6σ detections at the observed-frame fiducial wavelengths. This is a compromise to the dimming effects of redshift without entering a regime where the reduced S/N dominates the results. We do not consider the Ns instrument as we found it provides no meaningful constraints on luminosities at $z \gg 0.1$.

The results are shown in Figures 8 and 9, and in Table A1. For $L_{\rm Tot}$, Ms and NMp give luminosities that are biased low by about 50% at all redshifts. The high- (low-) PAH EW simulations predict more (less) bias, respectively. In contrast, Fs gives measures of $L_{\rm Tot}$ that are virtually unbiased across all redshifts, and shows no significant difference between the high- and low-PAH EW subsamples. The Fp instrument gives

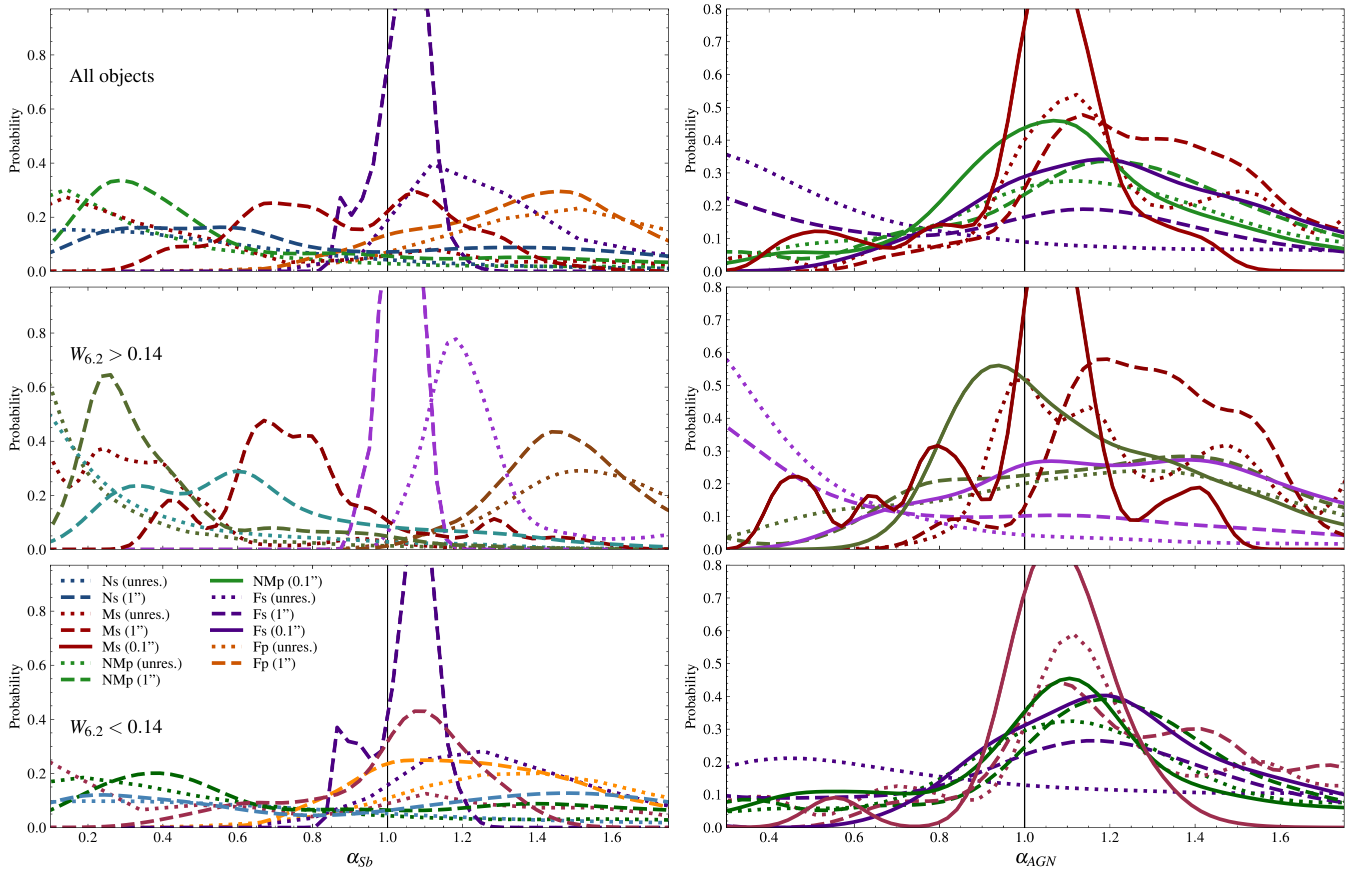

Figure 7. The effect on the recovery of (left column) starburst and (right column) AGN luminosity of observing at 1″ angular resolution for L_{Sb}, and 1″ and 0.″1 resolution for L_{AGN} (Section 6.1.4). The three rows show results for simulations using all objects, and the high-PAH EW and low-PAH EW subsamples. The results for Ns and Fp are not plotted as the finer angular resolution does not change their results significantly.

L_{Tot} estimates that are biased high at lower redshifts, but this bias reduces to nearly zero by $z \sim 5$. For L_{Sb}, we obtain similar results as for L_{Tot}: Ms and NMp give luminosities that are biased low by about 50% at most redshifts, Fs gives almost unbiased results, and Fp is biased high at most redshifts. For L_{AGN}, Ms and NMp observations at low redshift have small systematic bias, but the bias becomes more negative as redshift increases. In contrast, the L_{AGN} recovery with Fs is systematically biased low at low redshifts, but this bias diminishes as redshift increases. In all three cases, the low-PAH EW simulations again show less systematic bias than the high-PAH EW simulations. Observations with Fp give L_{AGN} values that are systematically biased low at all redshifts, and with large random errors.

We next examine how finer angular resolution affects the recovery of L_{Sb} and L_{AGN} as a function of redshift. The results are shown in Figures 10 and 11, and in Table A1. Finer angular resolution improves the recovery of L_{Sb} and L_{AGN} for all instruments at all redshifts. For L_{Sb}, arcsecond resolution significantly reduces, though does not eliminate, the systematic bias seen for Ms and Fp. There is only a small impact on the recovery with Fs or NMp. For L_{AGN}, there is noticeable improvement in recovery at 1″ resolution for Ms, NMp, and Fs, and substantial improvement at 0.″1 resolution. We do not obtain useful constraints on L_{AGN} with Fp at any angular resolution. As with Section 6.1.4, these results are lower bounds on the improvement from observing at finer angular resolution, due to our neglecting source confusion.

6.3. Observations with Multiple Instruments

6.3.1. Nearby Universe

We here examine luminosity recovery using combinations of the instruments in Table 2. We start at $z \sim 0.1$, assume detections at 10σ significance at the relevant fiducial wavelength, and include observations with Opt in all cases. To keep the simulations computationally reasonable, we do not consider the effects of observing at finer angular resolution.

The results are presented in Figure 12 and Table A2. The best recovery of luminosities is achieved with instruments that have a long wavelength baseline, and/or dense wavelength sampling. For L_{Tot}, the best recovery is achieved with instrument combinations that include Fs or Fp, especially Fs. Using Fs or Fp gives much better recovery than using Sp with the same shorter-wavelength instruments. Combinations with only photometric far-infrared observations overestimate L_{Tot}, while combinations with no far-infrared constraints underestimate L_{Tot}. We find similar results for the recovery of L_{Sb}. For L_{AGN}, the best results are obtained for combinations that include Ns and Ms, or NMp, plus one of Fs or Fp. Combinations without a far-infrared constraint tend to bias high, whereas combinations with poor mid-infrared constraints tend to bias low. For L_{H}, the best recovery is obtained with the inclusion of Ns and/or Fs, though in all cases the recovered host luminosities are biased low. While there are some minor variations, we obtain similar results when considering the high- or low-PAH EW simulations (Figure 13).

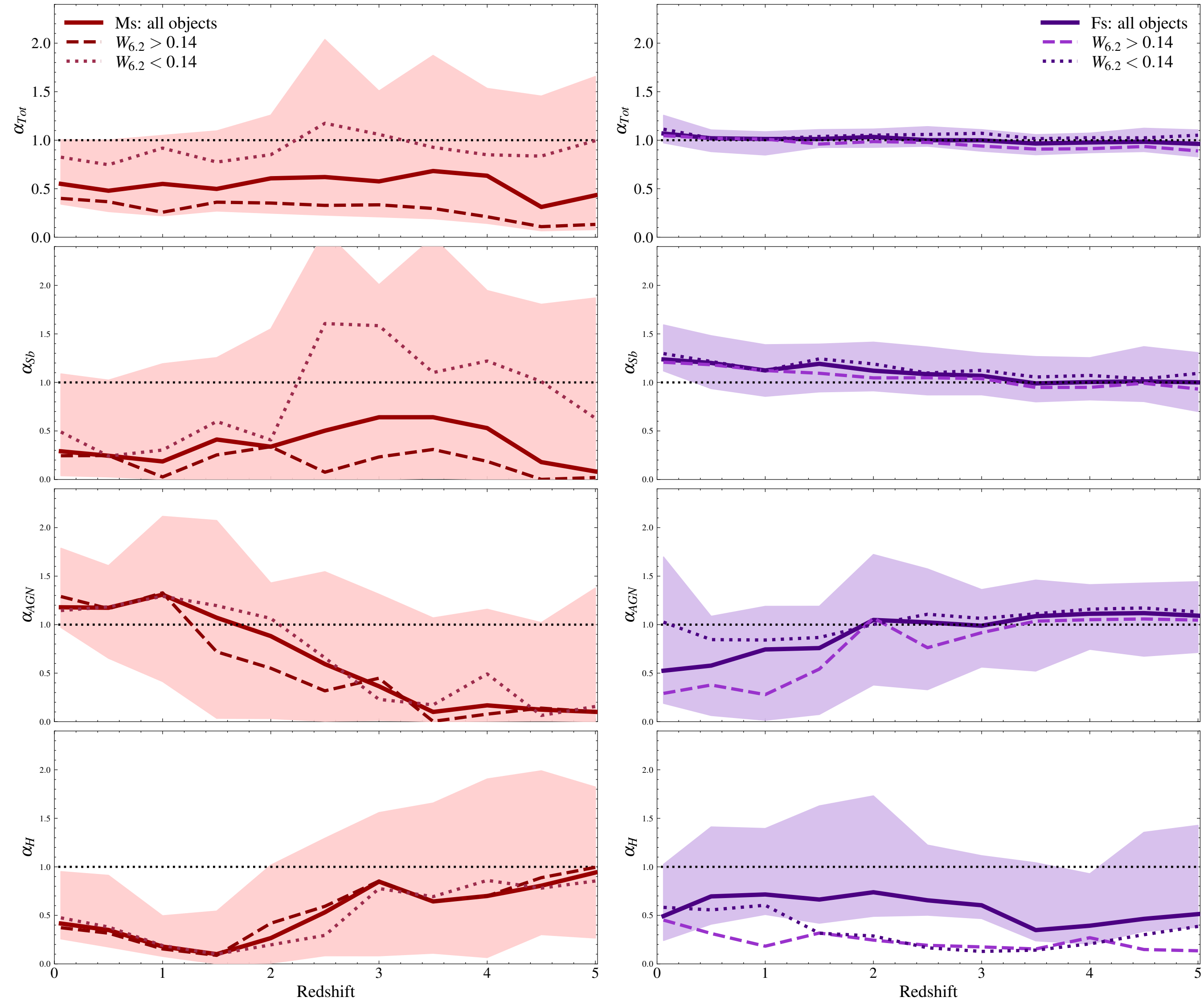

Figure 8. The recovery of total, starburst, AGN, and host-galaxy luminosity using (left column) Ms and (right column) Fs, over $0 < z < 5$ (Section 6.2). The solid line and shaded region show the results from simulations using all objects and the 1σ error region, The dashed and dotted lines show the results for the high- and low-PAH EW subsamples.

6.3.2. High-redshift Universe

Next, we examine the recovery of total and component luminosities using combinations of instruments over $0 < z < 5$. We consider two groups, one in which Ms is paired with longer-wavelength instruments (Figure 14), and one where NMp is paired with longer-wavelength instruments (Figure 15). We assume all observations have an S/N of 6 at their fiducial wavelengths. First considering the Ms group, the positive effects of wavelength sampling and coverage are evident. The addition of any of Fs, Fp, or Sp enhances the recovery of luminosities compared to Ms alone. However, the greatest enhancement is given by Fs, even though its wavelength baseline is shorter than Fp or Sp. Ms+Fs gives almost unbiased recovery of $L_{\rm Tot}$, $L_{\rm Sb}$, and $L_{\rm AGN}$ over most redshifts. Also notable is that Ms+Fp outperforms Ms+Sp. Turning to the NMp group, we obtain similar results, though with larger random errors.

Finally, we examine the efficacy of Ns in combinations of instruments observing over $0 < z < 5$ (Figure 16). At most redshifts, the inclusion of Ns observations does not significantly enhance the recovery of total or component luminosities.

7. Discussion and Conclusions

We have studied the recovery of rest-frame 1–1000 μm total, starburst, AGN, and host luminosities of infrared-luminous galaxies via SED fitting of photometric and low-resolution spectroscopic data. We have considered six fiducial near- to far-infrared instruments with real-world analogs, but have kept the simulations agnostic to specific facilities or survey designs.

7.1. Luminosity Recovery

The recovery of total and component luminosities of infrared-luminous galaxies depends on several interlinked factors. For $L_{\rm Tot}$, bias is minimized with observations over the broadest possible wavelength range. Spectroscopic, rather than photometric, coverage helps to minimize random error. For

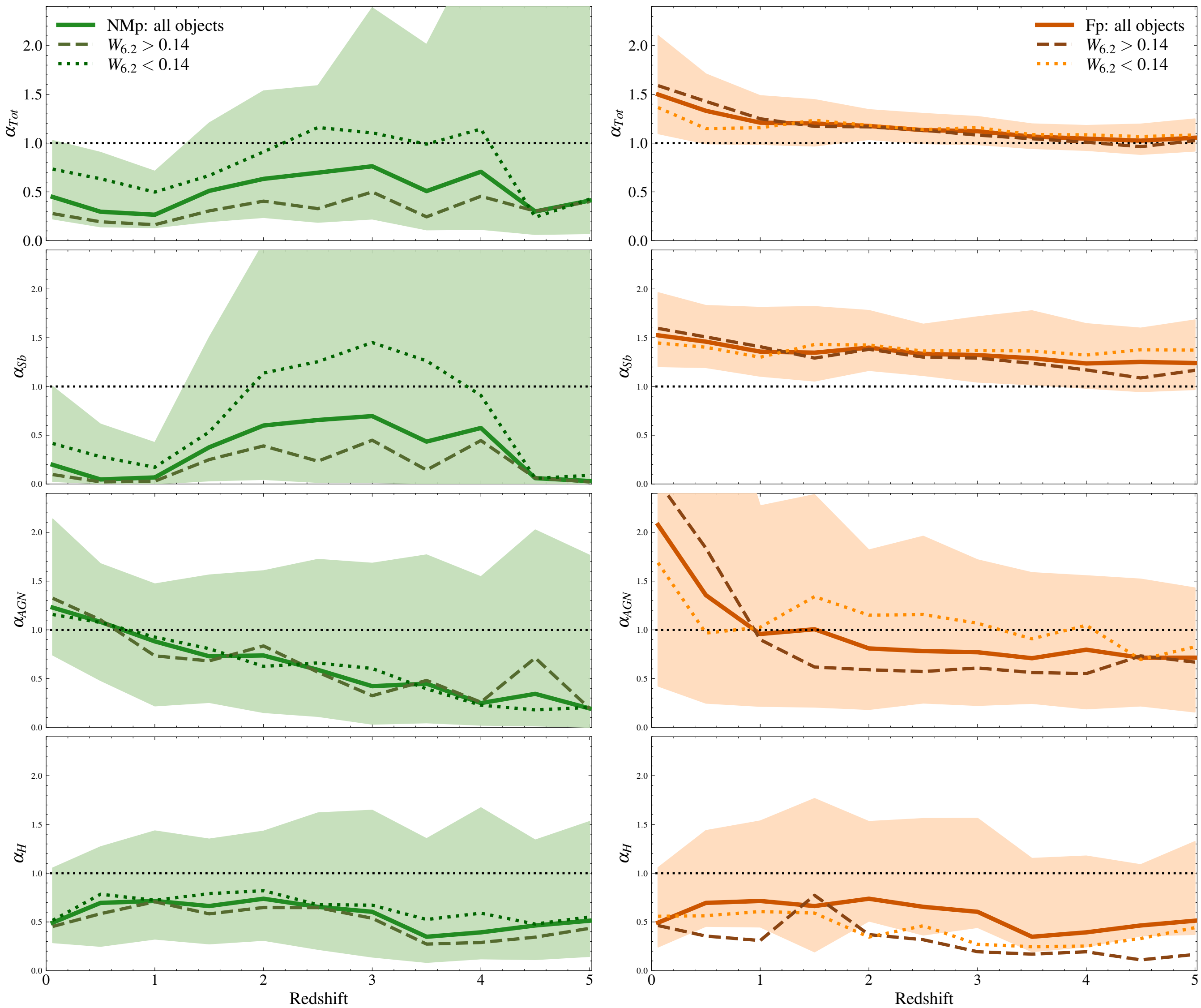

Figure 9. As Figure 8 but for the (left column) NMp and (right column) Fp instruments.

determining starburst, AGN, and host luminosities, the primary requirement is dense wavelength sampling where the component SED peaks: in the far-infrared for starburst, mid-infrared for AGN, and near-infrared for host. These wavelengths also correspond to where each component shows the greatest range in SED shapes. Thus, observations with different instruments will give different levels of accuracy and precision in recovered luminosities. Observations at far-infrared wavelengths will recover starburst luminosities that are either unbiased or biased high, but recover AGN luminosities that are biased low. Observations that favor mid-infrared wavelengths will give the opposite: unbiased or slightly high-biased AGN luminosities, and starburst luminosities that are biased low. However, while we find that starburst and AGN luminosities can be recovered with minimal bias using appropriate observations, the recovered host-galaxy luminosities are almost always biased low, by a factor of about 2 on average. A conceptually similar result has been found in previous studies (P. D. Mitchell et al. 2013; R. Sorba & M. Sawicki 2015; J. I. H. Li et al. 2021). We ascribe this to the challenge of measuring a faint host SED against the much brighter starburst/AGN SEDs.

The specific instruments that give the best luminosity recoveries depend on several factors. For a randomly selected source at $z \lesssim 0.1$, the best recovery of starburst luminosity is given by observations that include those at far-infrared wavelengths, especially those with dense wavelength sampling. For AGN luminosity, the best recovery is achieved with mid-infrared observations, with dense wavelength sampling again having a positive effect. Host-galaxy luminosities are best recovered with observations that include the near-infrared, though with the persistent low bias noted above. If the source is selected to be starburst (AGN) dominated, then the observations needed to achieve the least biased recovery of luminosities do not change, but the level of bias in the recovery does. Starburst (AGN)-dominated systems (as distinguished on the basis of 6.2 μm PAH EW; see Section 6.1.3) tend to show more (less) systematic bias for all of starburst, AGN, and host luminosity. The typical change in systematic bias relative to a randomly selected object is about 20% in both cases.

The S/N of the observations plays a significant role. With S/N $\lesssim 6$, the precision starts to degrade, with accuracy starting to degrade at S/N $\lesssim 4$. With S/Ns of 6–10, the accuracy and

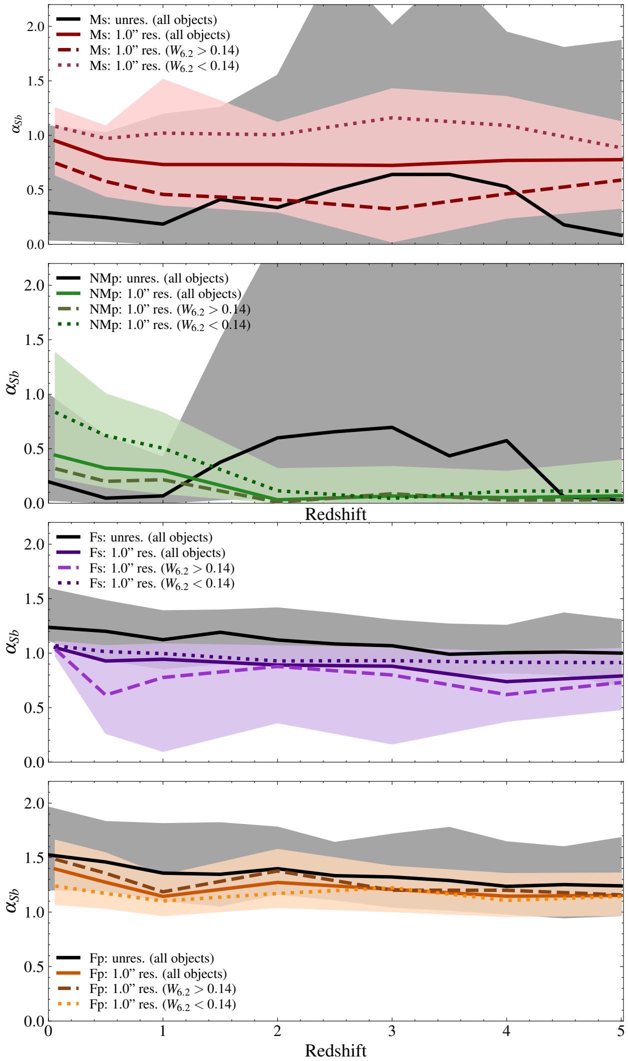

Figure 10. The effect of angular resolution on the recovery of starburst luminosity as a function of redshift, using the Ms, NMp, Fs, and Fp instruments (Section 6.2). Each panel compares the spatially unresolved results using all objects for starburst luminosity from Figure 8 with those obtained from observing at 1."0 resolution using all objects, and the high- and low-PAH EW subsamples.

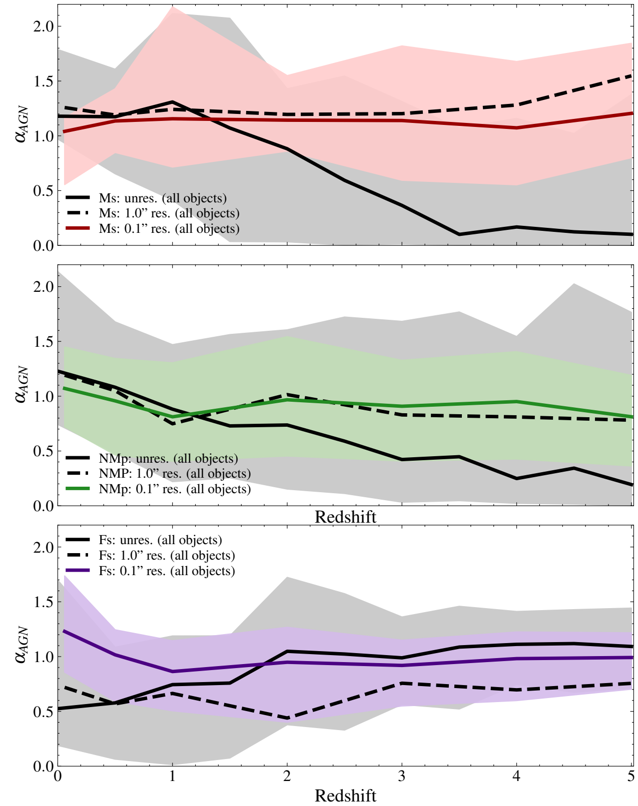

Figure 11. The effect of angular resolution on the recovery of AGN luminosity as a function of redshift, using the Ms, NMp, and Fs instruments (Section 6.2). Each panel compares the spatially unresolved results using all objects for AGN luminosity from Figure 8 with those obtained from observing at 1."0 and 0."1 resolution using all objects (the results for the high- and low-PAH EW subsamples are omitted as they lie close to their respective results using all objects).

precision both improve, and with S/Ns of 10–20 there is little change in either.

Angular resolution also plays an important role. Compared to the unresolved case, observing at (sub)arcsecond resolution reduces both systematic bias and random error for all mid- through far-infrared observations. Starburst luminosities can be recovered with almost no systematic bias with mid-infrared observations, while AGN luminosity recovery becomes feasible with far-infrared observations, albeit only those with dense wavelength sampling. Since we neglect source confusion, the true benefit of observing at finer angular resolution is likely greater than we present here.

When considering the recovery of total and component luminosities as a function of redshift, we obtain broadly similar results, with mid-infrared observations most useful for AGN luminosity and far-infrared observations most useful for starburst luminosity. However, these trends evolve with redshift. AGN luminosity recovery using observed-frame mid-infrared observations becomes progressively more biased low as redshift increases. Starburst luminosity recovery with far-infrared observations, however, shows much less increase in systematic bias, at least up to $z \sim 5$. Furthermore, as redshift increases, far-infrared observations become progressively better at measuring AGN luminosity. At most redshifts, we again see that starburst-dominated systems show more biased luminosity recovery than do AGN-dominated systems.

A potentially significant simplification in our analysis was the exclusion of mid- to far-infrared fine-structure lines that are commonly observed in luminous infrared galaxy spectra (primarily those from neon, sulfur, oxygen, nitrogen, and carbon) from the input SEDs to the simulations. Since these lines are not present in the SEDs we fit to the simulated data, their inclusion in the input SEDs would have some impact on our results. We defer an analysis of this scenario to a future work, and here only briefly speculate on the magnitude of this impact. For the spectrographs (Ns, Ms, and Fs) the impact is likely insignificant as the regions of continuum that contain these lines can be identified and removed. However, for the NMp and Fp instruments this is not possible, so the impact will be larger. There will be some systematic bias high (since the fits would ascribe the line and continuum flux to continuum) with additional random error caused by variation in line strengths for a given starburst or AGN luminosity. We speculate, though, based on typical line luminosity-to-total infrared luminosity ratios of our sample (D. Farrah et al. 2007, 2013), that the magnitude of both effects is of order 10% or less.

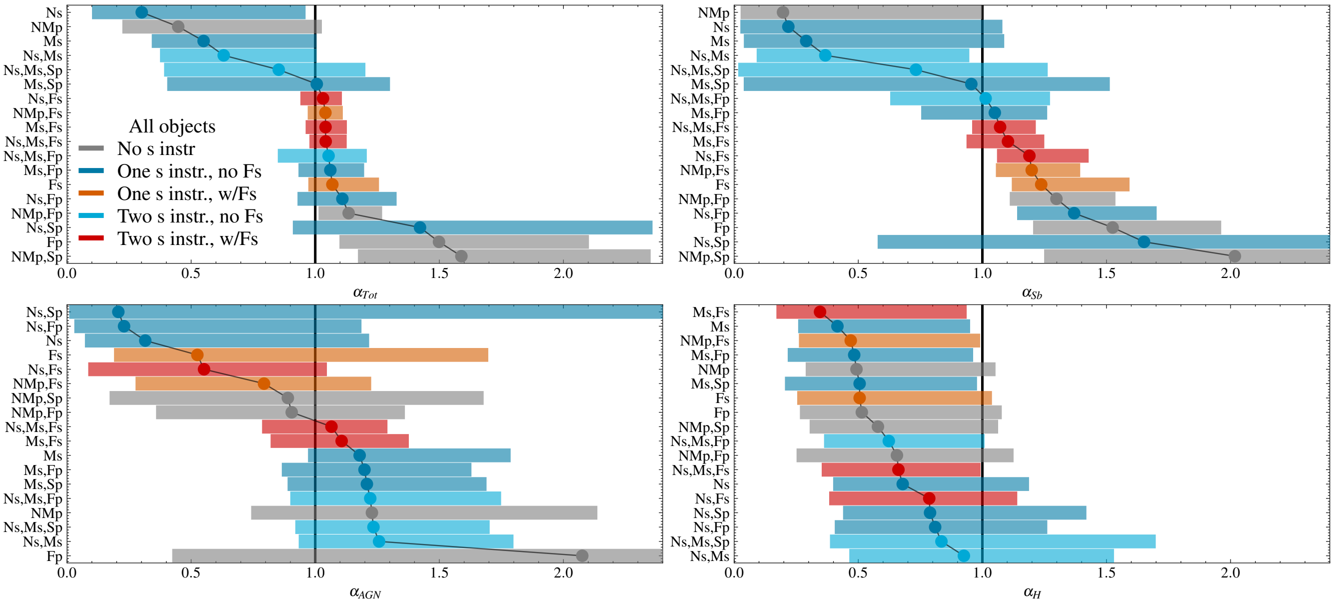

Figure 12. The recovery of total, starburst, AGN, and host luminosity at $z \sim 0.1$, using the combinations of instruments specified on the y-axis (Section 6.3). In each panel, the results are ordered by their α value. The error bars are the 1σ uncertainties.

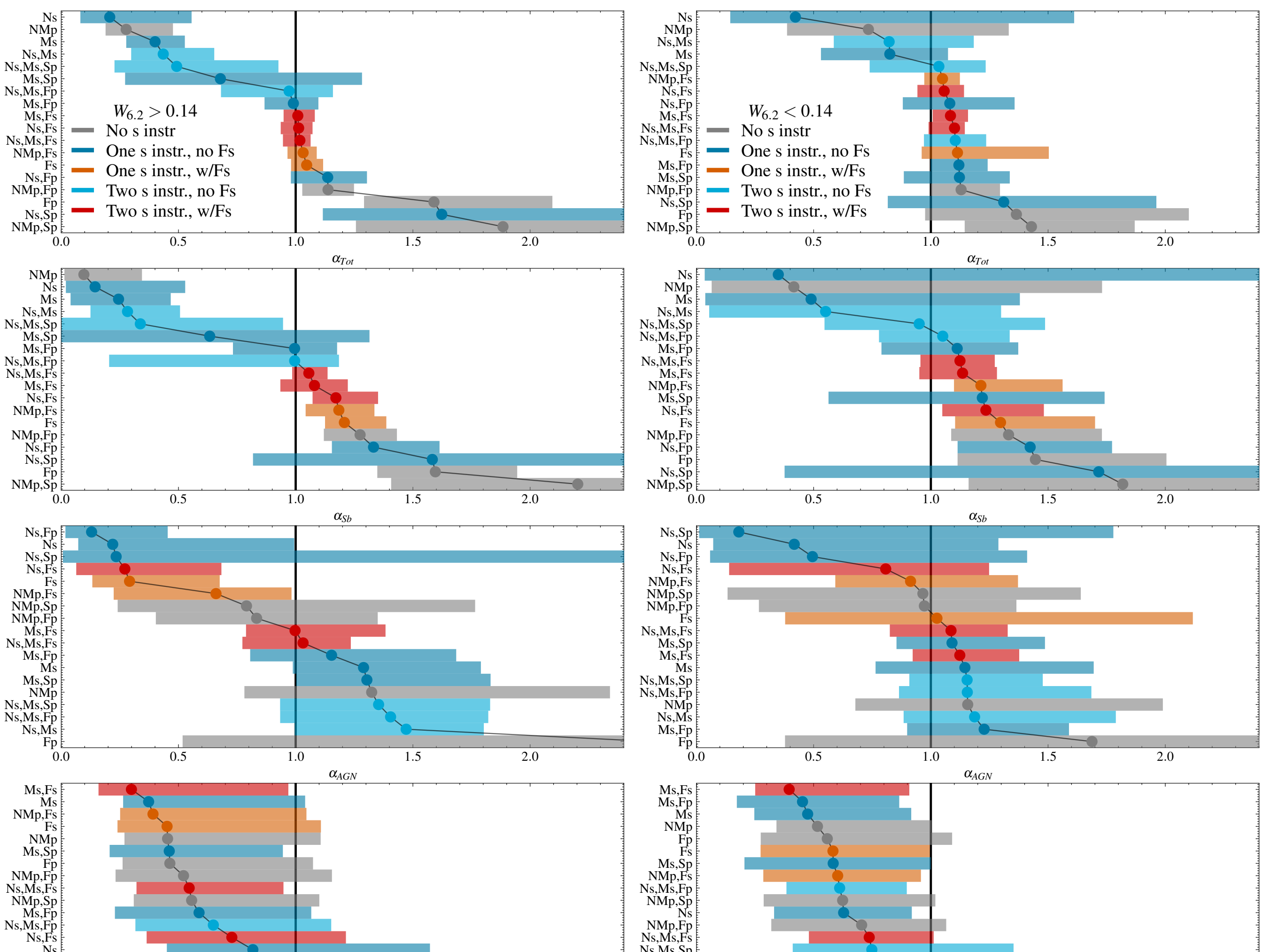

Figure 13. As Figure 12 but for the (top rows) high-PAH EW and (bottom rows) low-PAH EW subsamples.

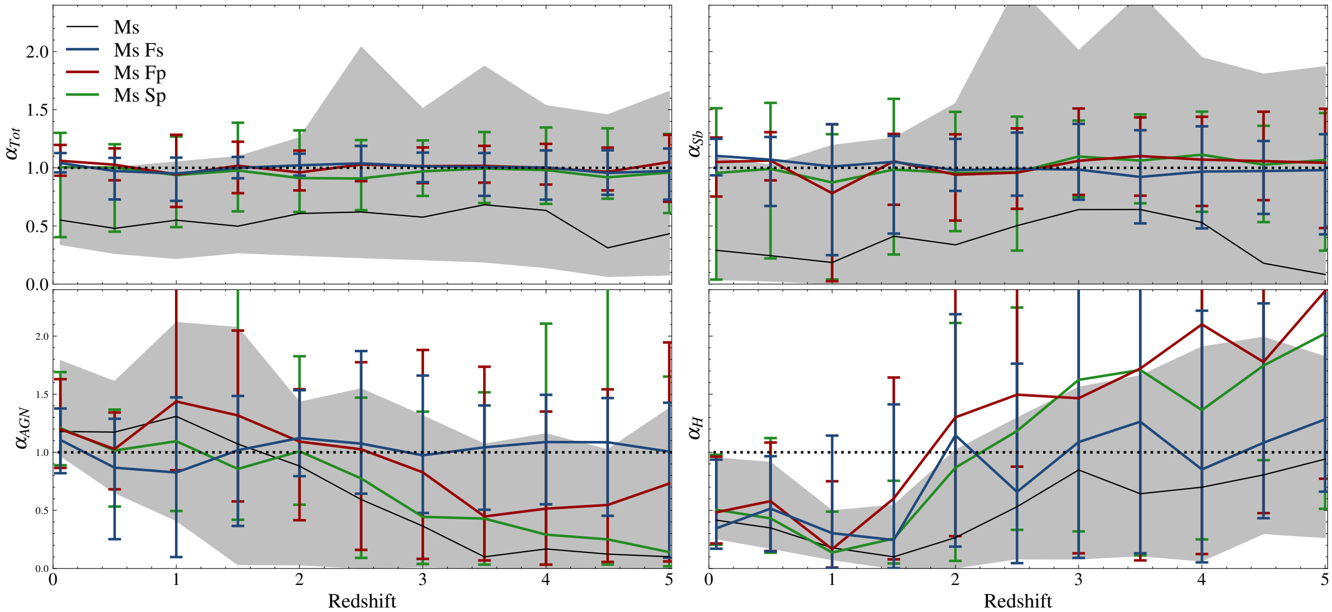

Figure 14. The recovery of total, starburst, AGN, and host luminosity as a function of redshift, using combinations of instruments where one of those instruments is Ms (Section 6.3). The recovery using Ms alone is included for comparison.

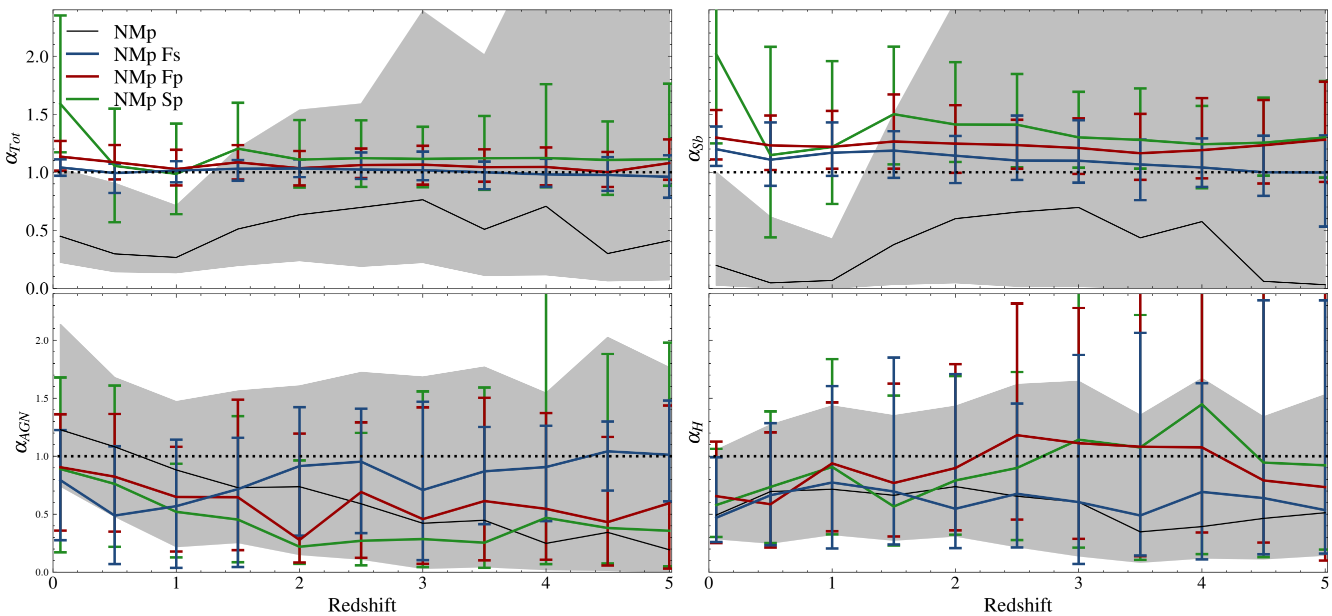

Figure 15. The recovery of total, starburst, AGN, and host luminosity as a function of redshift, using combinations of instruments where one of those instruments is NMp (Section 6.3). The recovery using NMp alone is included for comparison.

7.2. Implications for Future Work

Several implications follow from these results. First, studies that aim to calibrate quantities such as an infrared color, or the flux of a mid- or far-infrared line, as a measure of luminosity will be systematically biased unless the luminosities used to perform the calibration adhere to the requirements described above. This is especially relevant for estimating the infrared luminosities of the $z \gtrsim 4$ systems found by JWST, for which using calibrated relations is currently the only realistic route. It is likely also important that the population used to calibrate a line relation is similar in nature to the object under study. Second is the outlook for future near- through far-infrared observatories. Our results show the importance of dense wavelength sampling, as well as wavelength coverage, at any wavelength. They also showcase the potentially transformative power of a far-infrared instrument with either multiple photometric bands, or, to an even greater degree, one that observes continuously from 20–30 μm to 200–300 μm. Such an instrument reduces systematic bias and random error on the recovery of total and starburst luminosity over mid-infrared spectroscopy by at least a factor of 4, and substantially enhances the recovery of AGN and host luminosity in conjunction with other instruments. Either a multiband far-infrared photometer or spectrometer covering a broad wavelength range is substantially better at recovering unbiased starburst and AGN luminosities than ground-based

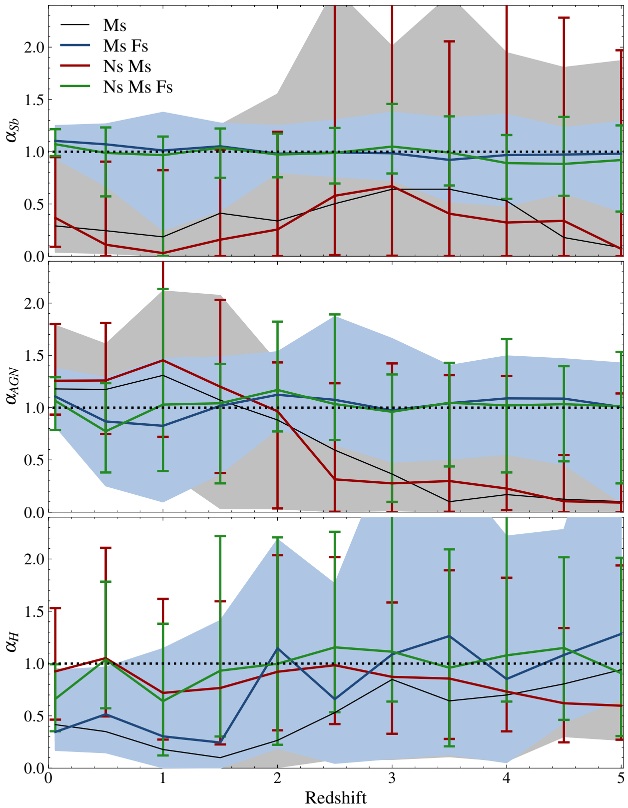

Figure 16. The effect of including Ns observations on the recovery of component luminosities as a function of redshift, if Ms observations are already present (Section 6.3).

submillimeter observations, at all redshifts. Examples of such far-infrared facilities include the SPIRIT interferometer, and the FIRESS and PRIMAger instruments on board PRIMA.

Acknowledgments

I.S. acknowledges funding from the European Research Council (ERC) DistantDust (grant No. 101117541) and the Atraccíon de Talento grant No. 2022-T1/TIC-20472 of the Comunidad de Madrid, Spain. M.B. acknowledges support from the INAF minigrant "A systematic search for ultra-bright high-z strongly lensed galaxies in Planck catalogs." D.L.C. acknowledges support from the UK Space Agency/STFC grant No. ST/Y006097/1. E.H. gratefully acknowledges the hospitality of the IAC during her long research visit and while this paper was being written. D.B.S. gratefully acknowledges support from NSF grant 2407752. The National Radio Astronomy Observatory and Green Bank Observatory are facilities of the U.S. National Science Foundation operated under cooperative agreement by Associated Universities, Inc. We thank River, John Petty, and Alaine Lee for useful discussions.

Appendix
True to Observed Ratios

We here present tables of the true-to-observed luminosity ratios derived and their 1σ uncertainties, for single-instrument (Table A1) and multi-instrument observations (Table A2).

Table A1
The Observed-to-true Ratios, α (Equation (1)), for Total, Starburst, AGN, and Host Luminosity Using Observations with Single Instruments

		Unresolved				1″.0		0″.1
Instrument	$W_{6.2}$	$\alpha_{\rm Tot}$	$\alpha_{\rm Sb}$	$\alpha_{\rm AGN}$	$\alpha_{\rm H}$	$\alpha_{\rm Sb}$	$\alpha_{\rm AGN}$	$\alpha_{\rm AGN}$
$z \sim 0$								
Ns	All	$0.30^{+0.66}_{-0.20}$	$0.22^{+0.86}_{-0.19}$	$0.32^{+0.90}_{-0.24}$	$0.68^{+0.51}_{-0.28}$	$0.74^{+0.84}_{-0.43}$	$0.06^{+1.14}_{-0.06}$	$0.41^{+0.88}_{-0.40}$
	>0.14	$0.21^{+0.35}_{-0.13}$	$0.14^{+0.38}_{-0.12}$	$0.22^{+0.77}_{-0.15}$	$0.82^{+0.76}_{-0.37}$	$0.61^{+0.48}_{-0.28}$	$0.01^{+0.38}_{-0.01}$	$0.24^{+0.66}_{-0.20}$
	<0.14	$0.42^{+1.19}_{-0.28}$	$0.35^{+2.30}_{-0.31}$	$0.42^{+0.87}_{-0.35}$	$0.63^{+0.29}_{-0.30}$	$1.21^{+0.57}_{-0.95}$	$0.38^{+1.03}_{-0.35}$	$0.75^{+0.75}_{-0.74}$
Ms	All	$0.55^{+0.46}_{-0.21}$	$0.29^{+0.80}_{-0.25}$	$1.18^{+0.61}_{-0.21}$	$0.42^{+0.53}_{-0.16}$	$0.95^{+0.30}_{-0.31}$	$1.26^{+0.29}_{-0.25}$	$1.04^{+0.13}_{-0.49}$
	>0.14	$0.40^{+0.13}_{-0.12}$	$0.24^{+0.22}_{-0.20}$	$1.29^{+0.50}_{-0.30}$	$0.37^{+0.67}_{-0.11}$	$0.75^{+0.28}_{-0.13}$	$1.31^{+0.23}_{-0.20}$	$1.04^{+0.11}_{-0.29}$
	<0.14	$0.82^{+0.25}_{-0.29}$	$0.49^{+0.89}_{-0.45}$	$1.15^{+0.55}_{-0.38}$	$0.47^{+0.44}_{-0.23}$	$1.08^{+0.20}_{-0.27}$	$1.15^{+0.43}_{-0.45}$	$1.04^{+0.13}_{-0.92}$
NMp	All	$0.45^{+0.58}_{-0.23}$	$0.20^{+0.80}_{-0.17}$	$1.23^{+0.91}_{-0.49}$	$0.49^{+0.56}_{-0.20}$	$0.44^{+0.94}_{-0.20}$	$1.19^{+0.43}_{-0.55}$	$1.07^{+0.38}_{-0.35}$
	>0.14	$0.28^{+0.20}_{-0.09}$	$0.10^{+0.25}_{-0.08}$	$1.32^{+1.02}_{-0.54}$	$0.45^{+0.65}_{-0.18}$	$0.32^{+0.34}_{-0.10}$	$1.28^{+0.49}_{-0.49}$	$1.09^{+0.39}_{-0.22}$
	<0.14	$0.73^{+0.60}_{-0.35}$	$0.42^{+1.31}_{-0.35}$	$1.16^{+0.83}_{-0.48}$	$0.52^{+0.49}_{-0.17}$	$0.83^{+0.91}_{-0.52}$	$1.15^{+0.34}_{-0.85}$	$1.06^{+0.35}_{-0.83}$
Fs	All	$1.07^{+0.19}_{-0.10}$	$1.24^{+0.36}_{-0.12}$	$0.53^{+1.17}_{-0.34}$	$0.51^{+0.53}_{-0.25}$	$1.05^{+0.06}_{-0.08}$	$0.72^{+0.73}_{-0.62}$	$1.23^{+0.51}_{-0.37}$
	>0.14	$1.05^{+0.07}_{-0.07}$	$1.21^{+0.18}_{-0.08}$	$0.29^{+0.38}_{-0.16}$	$0.45^{+0.66}_{-0.21}$	$1.04^{+0.05}_{-0.05}$	$0.35^{+0.83}_{-0.25}$	$1.35^{+0.61}_{-0.42}$
	<0.14	$1.11^{+0.39}_{-0.15}$	$1.30^{+0.40}_{-0.19}$	$1.03^{+1.09}_{-0.65}$	$0.58^{+0.41}_{-0.31}$	$1.07^{+0.05}_{-0.13}$	$1.08^{+0.52}_{-0.94}$	$1.17^{+0.39}_{-0.39}$
Fp	All	$1.50^{+0.60}_{-0.40}$	$1.52^{+0.44}_{-0.32}$	$2.08^{+4.57}_{-1.65}$	$0.51^{+0.56}_{-0.25}$	$1.40^{+0.26}_{-0.33}$	$1.11^{+1.98}_{-0.93}$	$0.97^{+0.74}_{-0.61}$
	>0.14	$1.59^{+0.51}_{-0.30}$	$1.60^{+0.35}_{-0.25}$	$2.52^{+4.96}_{-2.01}$	$0.46^{+0.61}_{-0.20}$	$1.48^{+0.22}_{-0.17}$	$1.45^{+2.44}_{-1.00}$	$0.96^{+0.71}_{-0.54}$
	<0.14	$1.36^{+0.74}_{-0.39}$	$1.45^{+0.56}_{-0.33}$	$1.69^{+4.30}_{-1.31}$	$0.56^{+0.53}_{-0.28}$	$1.24^{+0.34}_{-0.28}$	$0.85^{+1.54}_{-0.82}$	$0.97^{+0.80}_{-0.72}$
$z = 0.5$								
Ms	All	$0.48^{+0.52}_{-0.21}$	$0.24^{+0.78}_{-0.22}$	$1.17^{+0.43}_{-0.52}$	$0.35^{+0.56}_{-0.18}$	$0.79^{+0.30}_{-0.35}$	$1.19^{+0.56}_{-0.40}$	$1.14^{+0.29}_{-0.29}$
	>0.14	$0.37^{+0.14}_{-0.15}$	$0.25^{+0.20}_{-0.18}$	$1.16^{+0.47}_{-0.45}$	$0.32^{+0.67}_{-0.15}$	$0.58^{+0.24}_{-0.29}$	$1.23^{+0.52}_{-0.39}$	$1.17^{+0.36}_{-0.29}$
	<0.14	$0.75^{+0.34}_{-0.31}$	$0.24^{+1.08}_{-0.23}$	$1.18^{+0.40}_{-0.58}$	$0.38^{+0.45}_{-0.20}$	$0.97^{+0.20}_{-0.24}$	$1.19^{+0.56}_{-0.69}$	$1.12^{+0.23}_{-0.65}$
NMp	All	$0.30^{+0.61}_{-0.15}$	$0.05^{+0.57}_{-0.04}$	$1.08^{+0.60}_{-0.60}$	$0.70^{+0.58}_{-0.44}$	$0.32^{+0.68}_{-0.17}$	$1.05^{+0.69}_{-0.65}$	$0.96^{+0.39}_{-0.49}$
	>0.14	$0.19^{+0.10}_{-0.09}$	$0.02^{+0.05}_{-0.02}$	$1.10^{+0.68}_{-0.53}$	$0.58^{+0.86}_{-0.34}$	$0.20^{+0.49}_{-0.08}$	$0.97^{+0.71}_{-0.49}$	$0.97^{+0.46}_{-0.45}$
	<0.14	$0.63^{+0.57}_{-0.37}$	$0.28^{+1.10}_{-0.28}$	$1.08^{+0.49}_{-0.71}$	$0.78^{+0.45}_{-0.52}$	$0.62^{+0.77}_{-0.40}$	$1.11^{+0.74}_{-0.77}$	$0.94^{+0.37}_{-0.65}$
Fs	All	$1.02^{+0.09}_{-0.14}$	$1.20^{+0.28}_{-0.26}$	$0.58^{+0.51}_{-0.51}$	$0.46^{+0.72}_{-0.29}$	$0.93^{+0.14}_{-0.66}$	$0.57^{+0.88}_{-0.51}$	$1.02^{+0.23}_{-0.42}$
	>0.14	$1.02^{+0.07}_{-0.27}$	$1.18^{+0.21}_{-0.26}$	$0.38^{+0.49}_{-0.34}$	$0.31^{+0.70}_{-0.15}$	$0.62^{+0.40}_{-0.47}$	$0.18^{+0.85}_{-0.14}$	$0.94^{+0.27}_{-0.37}$
	<0.14	$1.02^{+0.12}_{-0.13}$	$1.22^{+0.35}_{-0.23}$	$0.85^{+0.40}_{-0.69}$	$0.56^{+0.67}_{-0.34}$	$1.01^{+0.07}_{-0.48}$	$0.86^{+0.70}_{-0.75}$	$1.05^{+0.21}_{-0.38}$
Fp	All	$1.33^{+0.38}_{-0.34}$	$1.46^{+0.37}_{-0.27}$	$1.36^{+2.70}_{-1.11}$	$0.46^{+0.74}_{-0.24}$	$1.27^{+0.27}_{-0.24}$	$1.84^{+3.09}_{-1.51}$	$0.94^{+1.10}_{-0.71}$
	>0.14	$1.43^{+0.28}_{-0.21}$	$1.51^{+0.32}_{-0.20}$	$1.84^{+2.96}_{-1.26}$	$0.36^{+0.81}_{-0.15}$	$1.36^{+0.23}_{-0.18}$	$2.30^{+3.25}_{-1.47}$	$0.74^{+1.12}_{-0.48}$
	<0.14	$1.15^{+0.55}_{-0.26}$	$1.40^{+0.43}_{-0.33}$	$0.97^{+2.01}_{-0.80}$	$0.56^{+0.67}_{-0.32}$	$1.17^{+0.30}_{-0.26}$	$1.30^{+2.93}_{-1.18}$	$1.14^{+1.04}_{-0.97}$
$z = 1$								
Ms	All	$0.55^{+0.50}_{-0.33}$	$0.19^{+1.01}_{-0.18}$	$1.31^{+0.81}_{-0.90}$	$0.18^{+0.32}_{-0.10}$	$0.73^{+0.78}_{-0.37}$	$1.24^{+1.48}_{-0.85}$	$1.16^{+1.02}_{-0.44}$
	>0.14	$0.26^{+0.18}_{-0.09}$	$0.03^{+0.24}_{-0.03}$	$1.33^{+0.63}_{-0.79}$	$0.15^{+0.17}_{-0.07}$	$0.46^{+0.48}_{-0.13}$	$1.17^{+1.33}_{-0.71}$	$1.15^{+1.01}_{-0.39}$
	<0.14	$0.92^{+0.39}_{-0.33}$	$0.30^{+1.45}_{-0.29}$	$1.29^{+0.88}_{-0.93}$	$0.19^{+0.58}_{-0.17}$	$1.02^{+0.72}_{-0.46}$	$1.41^{+1.31}_{-1.37}$	$1.19^{+1.10}_{-0.88}$
NMp	All	$0.27^{+0.45}_{-0.13}$	$0.07^{+0.36}_{-0.07}$	$0.88^{+0.59}_{-0.66}$	$0.72^{+0.72}_{-0.39}$	$0.30^{+0.53}_{-0.21}$	$0.75^{+0.72}_{-0.46}$	$0.81^{+0.49}_{-0.41}$
	>0.14	$0.16^{+0.14}_{-0.05}$	$0.03^{+0.14}_{-0.03}$	$0.73^{+0.81}_{-0.42}$	$0.71^{+0.87}_{-0.41}$	$0.22^{+0.15}_{-0.13}$	$0.78^{+0.81}_{-0.45}$	$0.79^{+0.54}_{-0.29}$
	<0.14	$0.50^{+0.51}_{-0.26}$	$0.17^{+0.81}_{-0.17}$	$0.93^{+0.49}_{-0.75}$	$0.72^{+0.51}_{-0.32}$	$0.50^{+0.55}_{-0.41}$	$0.72^{+0.69}_{-0.49}$	$0.85^{+0.44}_{-0.71}$
Fs	All	$1.01^{+0.07}_{-0.16}$	$1.12^{+0.26}_{-0.27}$	$0.74^{+0.44}_{-0.73}$	$0.28^{+0.68}_{-0.21}$	$0.94^{+0.14}_{-0.85}$	$0.66^{+0.65}_{-0.62}$	$0.86^{+0.28}_{-0.36}$
	>0.14	$1.01^{+0.09}_{-0.21}$	$1.12^{+0.18}_{-0.33}$	$0.28^{+0.69}_{-0.27}$	$0.18^{+0.33}_{-0.12}$	$0.78^{+0.27}_{-0.69}$	$0.21^{+0.71}_{-0.21}$	$0.82^{+0.17}_{-0.28}$
	<0.14	$1.01^{+0.07}_{-0.14}$	$1.12^{+0.33}_{-0.19}$	$0.84^{+0.42}_{-0.62}$	$0.60^{+0.62}_{-0.49}$	$1.00^{+0.13}_{-0.52}$	$0.94^{+0.57}_{-0.80}$	$0.99^{+0.17}_{-0.58}$
Fp	All	$1.21^{+0.28}_{-0.22}$	$1.36^{+0.45}_{-0.25}$	$0.96^{+1.31}_{-0.74}$	$0.42^{+0.82}_{-0.27}$	$1.14^{+0.19}_{-0.18}$	$1.14^{+1.75}_{-0.87}$	$0.98^{+1.15}_{-0.66}$
	>0.14	$1.25^{+0.21}_{-0.16}$	$1.41^{+0.40}_{-0.24}$	$0.90^{+1.21}_{-0.68}$	$0.31^{+0.48}_{-0.16}$	$1.19^{+0.18}_{-0.14}$	$1.13^{+1.83}_{-0.78}$	$0.80^{+1.06}_{-0.50}$
	<0.14	$1.16^{+0.41}_{-0.29}$	$1.30^{+0.52}_{-0.27}$	$1.03^{+1.34}_{-0.80}$	$0.61^{+0.82}_{-0.43}$	$1.10^{+0.19}_{-0.19}$	$1.15^{+1.66}_{-0.99}$	$1.12^{+1.16}_{-0.80}$
$z = 2$								
Ms	All	$0.61^{+0.65}_{-0.36}$	$0.34^{+1.21}_{-0.34}$	$0.88^{+0.55}_{-0.85}$	$0.27^{+0.75}_{-0.26}$	$0.73^{+0.39}_{-0.44}$	$1.20^{+0.44}_{-0.45}$	$1.14^{+0.41}_{-0.28}$
	>0.14	$0.35^{+0.50}_{-0.17}$	$0.34^{+0.54}_{-0.34}$	$0.55^{+0.65}_{-0.54}$	$0.42^{+0.81}_{-0.41}$	$0.41^{+0.13}_{-0.14}$	$1.18^{+0.59}_{-0.41}$	$1.14^{+0.43}_{-0.24}$
	<0.14	$0.85^{+0.73}_{-0.41}$	$0.41^{+1.83}_{-0.41}$	$1.06^{+0.44}_{-0.79}$	$0.20^{+0.67}_{-0.19}$	$1.01^{+0.19}_{-0.29}$	$1.20^{+0.37}_{-0.82}$	$1.14^{+0.29}_{-0.66}$
NMp	All	$0.63^{+0.90}_{-0.40}$	$0.60^{+1.87}_{-0.55}$	$0.74^{+0.87}_{-0.58}$	$0.74^{+0.69}_{-0.43}$	$0.03^{+0.28}_{-0.03}$	$1.01^{+0.71}_{-0.57}$	$0.97^{+0.58}_{-0.51}$
	>0.14	$0.40^{+0.36}_{-0.27}$	$0.39^{+0.48}_{-0.37}$	$0.83^{+0.93}_{-0.64}$	$0.65^{+0.99}_{-0.35}$	$0.01^{+0.05}_{-0.01}$	$1.01^{+0.88}_{-0.49}$	$1.03^{+0.57}_{-0.36}$
	<0.14	$0.91^{+1.40}_{-0.49}$	$1.14^{+2.88}_{-1.05}$	$0.63^{+0.86}_{-0.50}$	$0.82^{+0.49}_{-0.49}$	$0.11^{+0.48}_{-0.11}$	$1.02^{+0.61}_{-0.72}$	$0.92^{+0.56}_{-0.58}$
Fs	All	$1.03^{+0.08}_{-0.11}$	$1.12^{+0.29}_{-0.21}$	$1.05^{+0.67}_{-0.67}$	$0.27^{+0.99}_{-0.25}$	$0.89^{+0.18}_{-0.53}$	$0.44^{+0.94}_{-0.39}$	$0.95^{+0.32}_{-0.55}$
	>0.14	$0.99^{+0.10}_{-0.08}$	$1.05^{+0.21}_{-0.13}$	$1.07^{+2.01}_{-0.60}$	$0.25^{+0.87}_{-0.21}$	$0.88^{+0.13}_{-0.44}$	$0.22^{+0.51}_{-0.20}$	$0.84^{+0.26}_{-0.45}$
	<0.14	$1.05^{+0.08}_{-0.08}$	$1.19^{+0.45}_{-0.32}$	$1.00^{+0.52}_{-0.66}$	$0.29^{+1.10}_{-0.28}$	$0.93^{+0.17}_{-0.57}$	$0.90^{+0.85}_{-0.80}$	$1.06^{+0.32}_{-0.63}$
Fp	All	$1.18^{+0.17}_{-0.14}$	$1.40^{+0.38}_{-0.23}$	$0.81^{+1.01}_{-0.63}$	$0.35^{+0.79}_{-0.23}$	$1.27^{+0.30}_{-0.23}$	$1.72^{+3.21}_{-1.41}$	$1.01^{+1.16}_{-0.83}$

Table A1
(Continued)

Instrument	$W_{6.2}$	Unresolved				$1\farcs0$		$0\farcs1$
		$\alpha_{\rm Tot}$	$\alpha_{\rm Sb}$	$\alpha_{\rm AGN}$	$\alpha_{\rm H}$	$\alpha_{\rm Sb}$	$\alpha_{\rm AGN}$	$\alpha_{\rm AGN}$
	>0.14	$1.17^{+0.14}_{-0.13}$	$1.38^{+0.25}_{-0.19}$	$0.59^{+0.72}_{-0.43}$	$0.37^{+0.64}_{-0.21}$	$1.38^{+0.32}_{-0.21}$	$2.22^{+4.49}_{-1.73}$	$0.72^{+1.02}_{-0.54}$
	<0.14	$1.18^{+0.19}_{-0.15}$	$1.43^{+0.57}_{-0.30}$	$1.15^{+0.92}_{-0.94}$	$0.35^{+1.07}_{-0.25}$	$1.17^{+0.23}_{-0.24}$	$1.52^{+2.12}_{-1.34}$	$1.30^{+1.18}_{-1.14}$
$z=3$								
Ms	All	$0.58^{+0.93}_{-0.37}$	$0.64^{+1.37}_{-0.64}$	$0.36^{+0.95}_{-0.35}$	$0.85^{+0.71}_{-0.76}$	$0.72^{+0.70}_{-0.70}$	$1.20^{+0.89}_{-0.61}$	$1.14^{+0.68}_{-0.54}$
	>0.14	$0.33^{+0.42}_{-0.15}$	$0.23^{+0.74}_{-0.23}$	$0.45^{+0.91}_{-0.41}$	$0.85^{+0.66}_{-0.43}$	$0.32^{+0.45}_{-0.32}$	$1.37^{+0.76}_{-0.76}$	$1.41^{+0.69}_{-0.46}$
	<0.14	$1.06^{+1.42}_{-0.62}$	$1.58^{+1.78}_{-1.45}$	$0.23^{+1.05}_{-0.22}$	$0.78^{+0.93}_{-0.71}$	$1.16^{+0.54}_{-0.53}$	$1.16^{+0.28}_{-0.75}$	$1.03^{+0.36}_{-0.44}$
NMp	All	$0.76^{+1.63}_{-0.54}$	$0.70^{+2.61}_{-0.68}$	$0.42^{+1.26}_{-0.39}$	$0.60^{+1.04}_{-0.46}$	$0.07^{+0.27}_{-0.07}$	$0.83^{+0.65}_{-0.48}$	$0.91^{+0.42}_{-0.50}$
	>0.14	$0.50^{+0.84}_{-0.39}$	$0.45^{+1.02}_{-0.45}$	$0.32^{+1.36}_{-0.32}$	$0.54^{+0.83}_{-0.48}$	$0.09^{+0.19}_{-0.08}$	$0.76^{+0.66}_{-0.38}$	$0.86^{+0.52}_{-0.32}$
	<0.14	$1.11^{+1.66}_{-0.75}$	$1.45^{+2.63}_{-1.39}$	$0.60^{+1.09}_{-0.54}$	$0.67^{+1.07}_{-0.47}$	$0.04^{+0.41}_{-0.04}$	$0.91^{+0.58}_{-0.71}$	$0.96^{+0.34}_{-0.90}$
Fs	All	$1.00^{+0.11}_{-0.11}$	$1.07^{+0.23}_{-0.20}$	$0.99^{+0.37}_{-0.43}$	$0.17^{+0.51}_{-0.14}$	$0.88^{+0.17}_{-0.71}$	$0.76^{+0.88}_{-0.72}$	$0.92^{+0.23}_{-0.37}$
	>0.14	$0.94^{+0.08}_{-0.08}$	$1.04^{+0.16}_{-0.13}$	$0.92^{+0.27}_{-0.24}$	$0.17^{+0.28}_{-0.12}$	$0.80^{+0.21}_{-0.71}$	$0.62^{+0.86}_{-0.59}$	$0.88^{+0.21}_{-0.39}$
	<0.14	$1.07^{+0.08}_{-0.12}$	$1.13^{+0.36}_{-0.45}$	$1.06^{+0.52}_{-0.74}$	$0.13^{+1.18}_{-0.12}$	$0.93^{+0.14}_{-0.48}$	$0.80^{+0.95}_{-0.75}$	$0.99^{+0.18}_{-0.36}$
Fp	All	$1.12^{+0.15}_{-0.14}$	$1.32^{+0.39}_{-0.28}$	$0.77^{+0.95}_{-0.55}$	$0.23^{+0.96}_{-0.16}$	$1.21^{+0.21}_{-0.20}$	$1.11^{+2.02}_{-0.93}$	$1.17^{+1.10}_{-0.94}$
	>0.14	$1.08^{+0.13}_{-0.12}$	$1.29^{+0.22}_{-0.21}$	$0.61^{+0.62}_{-0.38}$	$0.19^{+0.35}_{-0.12}$	$1.20^{+0.16}_{-0.17}$	$1.31^{+2.03}_{-1.02}$	$0.98^{+1.40}_{-0.68}$
	<0.14	$1.16^{+0.18}_{-0.15}$	$1.37^{+0.66}_{-0.43}$	$1.07^{+1.01}_{-0.84}$	$0.27^{+2.18}_{-0.21}$	$1.22^{+0.27}_{-0.26}$	$0.97^{+1.84}_{-0.90}$	$1.24^{+1.00}_{-1.22}$
$z=4$								
Ms	All	$0.63^{+0.90}_{-0.49}$	$0.53^{+1.42}_{-0.53}$	$0.17^{+0.99}_{-0.16}$	$0.70^{+1.21}_{-0.63}$	$0.77^{+0.59}_{-0.53}$	$1.28^{+1.10}_{-0.82}$	$1.07^{+0.61}_{-0.52}$
	>0.14	$0.21^{+0.78}_{-0.12}$	$0.19^{+0.89}_{-0.18}$	$0.08^{+0.58}_{-0.08}$	$0.70^{+0.58}_{-0.54}$	$0.46^{+0.31}_{-0.30}$	$1.62^{+0.79}_{-1.21}$	$1.03^{+0.84}_{-0.37}$
	<0.14	$0.85^{+2.33}_{-0.56}$	$1.22^{+3.33}_{-1.22}$	$0.49^{+1.01}_{-0.47}$	$0.86^{+1.09}_{-0.83}$	$1.09^{+0.45}_{-0.50}$	$1.13^{+1.17}_{-0.66}$	$1.15^{+0.49}_{-0.92}$
NMp	All	$0.71^{+2.38}_{-0.59}$	$0.57^{+4.43}_{-0.57}$	$0.25^{+1.30}_{-0.23}$	$0.39^{+1.28}_{-0.27}$	$0.05^{+0.24}_{-0.05}$	$0.81^{+0.83}_{-0.56}$	$0.95^{+0.46}_{-0.52}$
	>0.14	$0.45^{+1.44}_{-0.36}$	$0.45^{+1.76}_{-0.45}$	$0.26^{+0.86}_{-0.26}$	$0.29^{+0.99}_{-0.19}$	$0.03^{+0.11}_{-0.03}$	$0.64^{+0.93}_{-0.38}$	$0.86^{+0.42}_{-0.38}$
	<0.14	$1.14^{+3.38}_{-1.01}$	$0.91^{+6.62}_{-0.91}$	$0.23^{+1.36}_{-0.19}$	$0.59^{+1.38}_{-0.38}$	$0.11^{+0.58}_{-0.11}$	$0.97^{+0.70}_{-0.75}$	$1.04^{+0.45}_{-0.78}$
Fs	All	$0.98^{+0.10}_{-0.11}$	$1.00^{+0.25}_{-0.18}$	$1.11^{+0.30}_{-0.37}$	$0.23^{+0.54}_{-0.19}$	$0.74^{+0.27}_{-0.36}$	$0.70^{+0.82}_{-0.68}$	$0.98^{+0.24}_{-0.38}$
	>0.14	$0.91^{+0.10}_{-0.07}$	$0.95^{+0.18}_{-0.13}$	$1.05^{+0.26}_{-0.29}$	$0.27^{+0.41}_{-0.20}$	$0.62^{+0.28}_{-0.54}$	$0.32^{+0.91}_{-0.31}$	$1.01^{+0.33}_{-0.44}$
	<0.14	$1.03^{+0.07}_{-0.09}$	$1.07^{+0.24}_{-0.25}$	$1.16^{+0.32}_{-0.72}$	$0.21^{+0.66}_{-0.19}$	$0.92^{+0.16}_{-0.40}$	$0.93^{+0.77}_{-0.82}$	$0.94^{+0.24}_{-0.31}$
Fp	All	$1.05^{+0.13}_{-0.12}$	$1.24^{+0.41}_{-0.25}$	$0.80^{+0.76}_{-0.61}$	$0.21^{+0.78}_{-0.15}$	$1.15^{+0.21}_{-0.19}$	$1.07^{+1.95}_{-0.90}$	$1.06^{+1.21}_{-0.83}$
	>0.14	$1.01^{+0.10}_{-0.13}$	$1.17^{+0.32}_{-0.18}$	$0.55^{+0.71}_{-0.39}$	$0.19^{+0.30}_{-0.13}$	$1.20^{+0.22}_{-0.19}$	$0.86^{+2.70}_{-0.63}$	$0.92^{+1.10}_{-0.71}$
	<0.14	$1.09^{+0.14}_{-0.12}$	$1.32^{+0.53}_{-0.36}$	$1.05^{+0.82}_{-0.79}$	$0.25^{+1.30}_{-0.18}$	$1.11^{+0.18}_{-0.19}$	$1.26^{+1.43}_{-1.15}$	$1.13^{+1.34}_{-0.89}$
$z=5$								
Ms	All	$0.43^{+1.22}_{-0.35}$	$0.08^{+1.79}_{-0.08}$	$0.10^{+1.28}_{-0.10}$	$0.94^{+0.88}_{-0.67}$	$0.78^{+0.35}_{-0.44}$	$1.55^{+0.99}_{-0.86}$	$1.20^{+0.64}_{-0.40}$
	>0.14	$0.13^{+0.52}_{-0.05}$	$0.02^{+0.72}_{-0.02}$	$0.10^{+0.91}_{-0.10}$	$1.00^{+2.26}_{-0.73}$	$0.59^{+0.41}_{-0.30}$	$1.56^{+0.81}_{-0.64}$	$1.16^{+0.67}_{-0.30}$
	<0.14	$1.00^{+1.93}_{-0.74}$	$0.63^{+4.06}_{-0.63}$	$0.16^{+3.58}_{-0.15}$	$0.85^{+0.93}_{-0.59}$	$0.89^{+0.37}_{-0.40}$	$1.54^{+1.33}_{-1.08}$	$1.26^{+1.01}_{-0.95}$
NMp	All	$0.41^{+2.95}_{-0.34}$	$0.03^{+3.01}_{-0.03}$	$0.19^{+1.57}_{-0.19}$	$0.51^{+1.02}_{-0.37}$	$0.07^{+0.33}_{-0.06}$	$0.78^{+0.56}_{-0.53}$	$0.81^{+0.38}_{-0.45}$
	>0.14	$0.40^{+1.83}_{-0.33}$	$0.02^{+2.11}_{-0.02}$	$0.19^{+2.76}_{-0.19}$	$0.43^{+1.22}_{-0.28}$	$0.03^{+0.15}_{-0.03}$	$0.83^{+0.61}_{-0.49}$	$0.75^{+0.32}_{-0.30}$
	<0.14	$0.43^{+3.50}_{-0.35}$	$0.09^{+4.96}_{-0.09}$	$0.20^{+1.31}_{-0.18}$	$0.55^{+0.83}_{-0.44}$	$0.11^{+0.46}_{-0.10}$	$0.76^{+0.44}_{-0.61}$	$0.93^{+0.38}_{-0.86}$
Fs	All	$0.96^{+0.14}_{-0.13}$	$1.00^{+0.31}_{-0.30}$	$1.09^{+0.35}_{-0.38}$	$0.19^{+0.91}_{-0.13}$	$0.79^{+0.25}_{-0.31}$	$0.76^{+0.59}_{-0.68}$	$0.99^{+0.23}_{-0.29}$
	>0.14	$0.89^{+0.10}_{-0.14}$	$0.93^{+0.17}_{-0.21}$	$1.05^{+0.38}_{-0.30}$	$0.14^{+0.26}_{-0.09}$	$0.73^{+0.14}_{-0.45}$	$0.53^{+0.62}_{-0.49}$	$1.02^{+0.21}_{-0.30}$
	<0.14	$1.05^{+0.13}_{-0.14}$	$1.09^{+0.29}_{-0.52}$	$1.13^{+0.34}_{-1.05}$	$0.39^{+1.73}_{-0.31}$	$0.91^{+0.19}_{-0.34}$	$0.94^{+0.56}_{-0.85}$	$0.98^{+0.23}_{-0.80}$
Fp	All	$1.06^{+0.19}_{-0.14}$	$1.24^{+0.44}_{-0.27}$	$0.71^{+0.72}_{-0.56}$	$0.21^{+0.81}_{-0.14}$	$1.15^{+0.20}_{-0.18}$	$1.32^{+2.48}_{-1.08}$	$1.15^{+0.89}_{-0.81}$
	>0.14	$1.03^{+0.18}_{-0.20}$	$1.17^{+0.26}_{-0.30}$	$0.67^{+0.54}_{-0.40}$	$0.17^{+0.37}_{-0.11}$	$1.16^{+0.16}_{-0.13}$	$1.26^{+2.84}_{-1.00}$	$1.10^{+1.06}_{-0.79}$
	<0.14	$1.08^{+0.18}_{-0.11}$	$1.37^{+0.71}_{-0.27}$	$0.83^{+0.68}_{-0.78}$	$0.44^{+0.80}_{-0.35}$	$1.14^{+0.25}_{-0.24}$	$1.33^{+2.27}_{-1.14}$	$1.18^{+0.79}_{-0.76}$

Note. Results are presented for $z \sim 0$, $z = 0.5$, $z = 1$, $z = 2$, $z = 3$, $z = 4$, and $z = 5$. For each redshift, results are presented for simulations using the entire input sample, and for high- and low-PAH 6.2 μm EW subsamples. For each of these samples, results are presented assuming the observations are spatially unresolved, and at angular resolutions of $1''$ for starburst and AGN, and $0\farcs1$ for AGN.

Table A2
The Observed-to-true Ratios, α (Equation (1)), for Total, Starburst, AGN, and Host Luminosity Using Observations with Multiple Instruments

Instruments	$W_{6.2}$	$\alpha_{\rm Tot}$	$\alpha_{\rm Sb}$	$\alpha_{\rm AGN}$	$\alpha_{\rm H}$
$z \sim 0$					
Ns Ms	All	$0.63^{+0.37}_{-0.26}$	$0.37^{+0.58}_{-0.28}$	$1.26^{+0.54}_{-0.32}$	$0.93^{+0.60}_{-0.46}$
	>0.14	$0.44^{+0.22}_{-0.14}$	$0.28^{+0.22}_{-0.16}$	$1.47^{+0.33}_{-0.48}$	$0.98^{+0.54}_{-0.48}$
	<0.14	$0.82^{+0.36}_{-0.24}$	$0.55^{+0.75}_{-0.50}$	$1.19^{+0.60}_{-0.30}$	$0.86^{+0.71}_{-0.43}$
Ns Fp	All	$1.11^{+0.22}_{-0.18}$	$1.37^{+0.33}_{-0.23}$	$0.23^{+0.96}_{-0.20}$	$0.81^{+0.45}_{-0.40}$
	>0.14	$1.14^{+0.17}_{-0.16}$	$1.33^{+0.28}_{-0.18}$	$0.13^{+0.32}_{-0.11}$	$0.83^{+0.56}_{-0.41}$
	<0.14	$1.08^{+0.28}_{-0.20}$	$1.42^{+0.35}_{-0.31}$	$0.50^{+0.92}_{-0.44}$	$0.80^{+0.32}_{-0.41}$
Ns Fs	All	$1.03^{+0.08}_{-0.09}$	$1.19^{+0.24}_{-0.13}$	$0.55^{+0.50}_{-0.47}$	$0.79^{+0.35}_{-0.40}$
	>0.14	$1.01^{+0.06}_{-0.08}$	$1.17^{+0.18}_{-0.10}$	$0.27^{+0.41}_{-0.21}$	$0.73^{+0.49}_{-0.36}$
	<0.14	$1.06^{+0.08}_{-0.11}$	$1.23^{+0.25}_{-0.19}$	$0.81^{+0.44}_{-0.67}$	$0.81^{+0.29}_{-0.42}$
Ns Sp	All	$1.42^{+0.94}_{-0.51}$	$1.65^{+0.77}_{-1.07}$	$0.21^{+3.52}_{-0.20}$	$0.79^{+0.63}_{-0.35}$
	>0.14	$1.62^{+1.04}_{-0.51}$	$1.58^{+0.83}_{-0.76}$	$0.23^{+6.34}_{-0.23}$	$0.82^{+0.91}_{-0.33}$
	<0.14	$1.31^{+0.65}_{-0.49}$	$1.72^{+0.70}_{-1.34}$	$0.18^{+1.60}_{-0.17}$	$0.77^{+0.34}_{-0.38}$
Ms Fp	All	$1.06^{+0.14}_{-0.13}$	$1.05^{+0.21}_{-0.30}$	$1.20^{+0.43}_{-0.33}$	$0.48^{+0.48}_{-0.27}$
	>0.14	$0.99^{+0.11}_{-0.12}$	$1.00^{+0.18}_{-0.26}$	$1.15^{+0.53}_{-0.35}$	$0.59^{+0.48}_{-0.36}$
	<0.14	$1.12^{+0.12}_{-0.12}$	$1.11^{+0.26}_{-0.32}$	$1.23^{+0.36}_{-0.33}$	$0.45^{+0.41}_{-0.28}$
Ms Fs	All	$1.04^{+0.09}_{-0.08}$	$1.10^{+0.15}_{-0.17}$	$1.11^{+0.27}_{-0.29}$	$0.35^{+0.59}_{-0.18}$
	>0.14	$1.01^{+0.07}_{-0.06}$	$1.08^{+0.14}_{-0.15}$	$1.00^{+0.39}_{-0.21}$	$0.30^{+0.67}_{-0.14}$
	<0.14	$1.08^{+0.07}_{-0.08}$	$1.14^{+0.15}_{-0.18}$	$1.12^{+0.25}_{-0.20}$	$0.40^{+0.51}_{-0.14}$
Ms Sp	All	$1.01^{+0.30}_{-0.60}$	$0.96^{+0.56}_{-0.92}$	$1.21^{+0.48}_{-0.32}$	$0.51^{+0.47}_{-0.30}$
	>0.14	$0.68^{+0.60}_{-0.41}$	$0.63^{+0.68}_{-0.63}$	$1.30^{+0.53}_{-0.30}$	$0.46^{+0.48}_{-0.25}$
	<0.14	$1.12^{+0.21}_{-0.24}$	$1.22^{+0.52}_{-0.66}$	$1.09^{+0.40}_{-0.24}$	$0.58^{+0.42}_{-0.38}$
NMp Fp	All	$1.13^{+0.13}_{-0.12}$	$1.30^{+0.24}_{-0.19}$	$0.91^{+0.46}_{-0.55}$	$0.66^{+0.47}_{-0.40}$
	>0.14	$1.14^{+0.11}_{-0.11}$	$1.27^{+0.16}_{-0.15}$	$0.83^{+0.52}_{-0.43}$	$0.52^{+0.63}_{-0.29}$
	<0.14	$1.13^{+0.17}_{-0.13}$	$1.33^{+0.40}_{-0.24}$	$0.97^{+0.39}_{-0.71}$	$0.70^{+0.36}_{-0.39}$
NMp Fs	All	$1.04^{+0.07}_{-0.07}$	$1.20^{+0.20}_{-0.14}$	$0.79^{+0.43}_{-0.52}$	$0.47^{+0.52}_{-0.21}$
	>0.14	$1.03^{+0.06}_{-0.07}$	$1.18^{+0.15}_{-0.14}$	$0.66^{+0.32}_{-0.44}$	$0.39^{+0.65}_{-0.14}$
	<0.14	$1.05^{+0.07}_{-0.08}$	$1.21^{+0.35}_{-0.11}$	$0.91^{+0.46}_{-0.32}$	$0.60^{+0.36}_{-0.32}$
NMp Sp	All	$1.59^{+0.76}_{-0.42}$	$2.02^{+0.92}_{-0.77}$	$0.89^{+0.79}_{-0.72}$	$0.58^{+0.48}_{-0.28}$
	>0.14	$1.88^{+0.76}_{-0.63}$	$2.20^{+0.96}_{-0.80}$	$0.79^{+0.98}_{-0.55}$	$0.56^{+0.54}_{-0.25}$
	<0.14	$1.43^{+0.44}_{-0.28}$	$1.82^{+0.82}_{-0.66}$	$0.97^{+0.67}_{-0.83}$	$0.62^{+0.40}_{-0.34}$
Ns Ms Fp	All	$1.05^{+0.15}_{-0.20}$	$1.01^{+0.26}_{-0.38}$	$1.22^{+0.53}_{-0.32}$	$0.62^{+0.39}_{-0.26}$
	>0.14	$0.97^{+0.19}_{-0.29}$	$1.00^{+0.19}_{-0.79}$	$1.40^{+0.42}_{-0.47}$	$0.65^{+0.50}_{-0.33}$
	<0.14	$1.10^{+0.13}_{-0.13}$	$1.05^{+0.29}_{-0.27}$	$1.16^{+0.53}_{-0.29}$	$0.61^{+0.29}_{-0.23}$
Ns Ms Fs	All	$1.04^{+0.08}_{-0.07}$	$1.07^{+0.14}_{-0.11}$	$1.07^{+0.23}_{-0.28}$	$0.66^{+0.33}_{-0.31}$
	>0.14	$1.02^{+0.05}_{-0.07}$	$1.06^{+0.08}_{-0.07}$	$1.03^{+0.20}_{-0.26}$	$0.55^{+0.40}_{-0.22}$
	<0.14	$1.10^{+0.04}_{-0.11}$	$1.12^{+0.15}_{-0.17}$	$1.09^{+0.24}_{-0.26}$	$0.74^{+0.27}_{-0.26}$
Ns Ms Sp	All	$0.85^{+0.35}_{-0.46}$	$0.73^{+0.53}_{-0.72}$	$1.23^{+0.47}_{-0.31}$	$0.84^{+0.86}_{-0.45}$
	>0.14	$0.49^{+0.43}_{-0.27}$	$0.34^{+0.61}_{-0.34}$	$1.35^{+0.48}_{-0.42}$	$1.06^{+0.82}_{-0.73}$
	<0.14	$1.03^{+0.20}_{-0.30}$	$0.95^{+0.54}_{-0.40}$	$1.15^{+0.32}_{-0.25}$	$0.75^{+0.60}_{-0.34}$
$z = 0.5$					
Ms Fs	All	$0.97^{+0.11}_{-0.25}$	$1.07^{+0.19}_{-0.40}$	$0.87^{+0.42}_{-0.62}$	$0.52^{+0.45}_{-0.37}$
	>0.14	$0.92^{+0.10}_{-0.78}$	$0.98^{+0.20}_{-0.98}$	$0.69^{+0.41}_{-0.47}$	$0.57^{+0.35}_{-0.43}$
	<0.14	$1.02^{+0.09}_{-0.09}$	$1.14^{+0.20}_{-0.28}$	$0.94^{+0.52}_{-0.65}$	$0.47^{+0.50}_{-0.31}$
Ms Fp	All	$1.03^{+0.14}_{-0.13}$	$1.06^{+0.24}_{-0.17}$	$1.03^{+0.32}_{-0.35}$	$0.58^{+0.50}_{-0.43}$
	>0.14	$0.98^{+0.12}_{-0.10}$	$1.03^{+0.21}_{-0.13}$	$0.96^{+0.29}_{-0.22}$	$0.73^{+0.42}_{-0.55}$
	<0.14	$1.07^{+0.13}_{-0.16}$	$1.10^{+0.25}_{-0.23}$	$1.10^{+0.44}_{-0.64}$	$0.42^{+0.63}_{-0.39}$
Ms Sp	All	$1.00^{+0.20}_{-0.55}$	$0.99^{+0.57}_{-0.77}$	$1.02^{+0.35}_{-0.48}$	$0.43^{+0.69}_{-0.30}$
	>0.14	$0.63^{+0.48}_{-0.26}$	$0.57^{+0.67}_{-0.35}$	$1.02^{+0.43}_{-0.48}$	$0.48^{+0.75}_{-0.35}$
	<0.14	$1.03^{+0.18}_{-0.25}$	$1.12^{+0.49}_{-0.82}$	$1.02^{+0.28}_{-0.64}$	$0.38^{+0.66}_{-0.23}$
NMp Fs	All	$0.99^{+0.08}_{-0.17}$	$1.11^{+0.32}_{-0.23}$	$0.49^{+0.60}_{-0.42}$	$0.66^{+0.62}_{-0.43}$
	>0.14	$0.97^{+0.09}_{-0.15}$	$1.08^{+0.19}_{-0.20}$	$0.36^{+0.48}_{-0.35}$	$0.68^{+0.39}_{-0.45}$
	<0.14	$1.01^{+0.07}_{-0.16}$	$1.15^{+0.47}_{-0.18}$	$0.68^{+0.63}_{-0.49}$	$0.66^{+0.68}_{-0.43}$
NMp Fp	All	$1.09^{+0.15}_{-0.15}$	$1.23^{+0.26}_{-0.21}$	$0.82^{+0.54}_{-0.47}$	$0.59^{+0.62}_{-0.37}$
	>0.14	$1.13^{+0.17}_{-0.16}$	$1.27^{+0.19}_{-0.24}$	$0.81^{+0.58}_{-0.49}$	$0.60^{+0.47}_{-0.39}$
	<0.14	$1.06^{+0.10}_{-0.16}$	$1.20^{+0.36}_{-0.19}$	$0.83^{+0.53}_{-0.43}$	$0.57^{+0.65}_{-0.34}$

Table A2
(Continued)

Instruments	$W_{6.2}$	$\alpha_{\rm Tot}$	$\alpha_{\rm Sb}$	$\alpha_{\rm AGN}$	$\alpha_{\rm H}$
NMp Sp	All	$1.05^{+0.49}_{-0.49}$	$1.15^{+0.93}_{-0.71}$	$0.76^{+0.85}_{-0.54}$	$0.74^{+0.65}_{-0.48}$
	>0.14	$0.94^{+0.58}_{-0.70}$	$1.04^{+0.65}_{-0.95}$	$0.72^{+0.77}_{-0.45}$	$0.80^{+0.69}_{-0.47}$
	<0.14	$1.18^{+0.38}_{-0.34}$	$1.39^{+0.86}_{-0.69}$	$0.88^{+0.95}_{-0.74}$	$0.68^{+0.63}_{-0.48}$
$z = 1$					
Ms Fs	All	$0.95^{+0.14}_{-0.24}$	$1.01^{+0.36}_{-0.76}$	$0.83^{+0.65}_{-0.73}$	$0.30^{+0.84}_{-0.30}$
	>0.14	$0.87^{+0.15}_{-0.18}$	$0.90^{+0.32}_{-0.79}$	$0.74^{+0.73}_{-0.58}$	$0.31^{+0.90}_{-0.24}$
	<0.14	$1.00^{+0.12}_{-0.21}$	$1.06^{+0.41}_{-0.58}$	$0.88^{+0.58}_{-0.85}$	$0.16^{+0.95}_{-0.16}$
Ms Fp	All	$0.94^{+0.34}_{-0.28}$	$0.78^{+0.59}_{-0.76}$	$1.44^{+1.85}_{-0.59}$	$0.17^{+0.58}_{-0.16}$
	>0.14	$0.83^{+0.23}_{-0.36}$	$0.74^{+0.42}_{-0.73}$	$1.88^{+1.80}_{-0.50}$	$0.24^{+0.53}_{-0.19}$
	<0.14	$1.12^{+0.20}_{-0.33}$	$1.15^{+0.34}_{-0.87}$	$1.20^{+1.71}_{-0.72}$	$0.11^{+0.60}_{-0.11}$
Ms Sp	All	$0.94^{+0.33}_{-0.45}$	$0.87^{+0.42}_{-0.83}$	$1.10^{+1.56}_{-0.60}$	$0.14^{+0.35}_{-0.14}$
	>0.14	$0.65^{+0.58}_{-0.34}$	$0.66^{+0.41}_{-0.49}$	$1.09^{+1.54}_{-0.60}$	$0.11^{+0.15}_{-0.11}$
	<0.14	$1.04^{+0.41}_{-0.19}$	$0.98^{+0.41}_{-0.97}$	$1.11^{+1.56}_{-0.74}$	$0.17^{+0.50}_{-0.17}$
NMp Fs	All	$1.01^{+0.08}_{-0.10}$	$1.17^{+0.26}_{-0.20}$	$0.57^{+0.57}_{-0.53}$	$0.77^{+0.83}_{-0.57}$
	>0.14	$1.01^{+0.07}_{-0.10}$	$1.16^{+0.13}_{-0.17}$	$0.42^{+0.54}_{-0.38}$	$0.47^{+1.05}_{-0.29}$
	<0.14	$1.03^{+0.08}_{-0.11}$	$1.18^{+0.43}_{-0.25}$	$0.78^{+0.39}_{-0.75}$	$0.96^{+0.65}_{-0.66}$
NMp Fp	All	$1.03^{+0.17}_{-0.14}$	$1.22^{+0.31}_{-0.19}$	$0.65^{+0.43}_{-0.47}$	$0.94^{+0.53}_{-0.59}$
	>0.14	$1.06^{+0.18}_{-0.14}$	$1.23^{+0.26}_{-0.20}$	$0.49^{+0.50}_{-0.30}$	$0.91^{+0.64}_{-0.69}$
	<0.14	$1.01^{+0.14}_{-0.15}$	$1.22^{+0.39}_{-0.18}$	$0.74^{+0.46}_{-0.57}$	$0.96^{+0.44}_{-0.48}$
NMp Sp	All	$0.99^{+0.43}_{-0.35}$	$1.22^{+0.74}_{-0.49}$	$0.52^{+0.41}_{-0.39}$	$0.91^{+0.93}_{-0.58}$
	>0.14	$1.09^{+0.39}_{-0.43}$	$1.23^{+0.70}_{-0.53}$	$0.43^{+0.36}_{-0.26}$	$0.77^{+1.34}_{-0.52}$
	<0.14	$0.94^{+0.38}_{-0.31}$	$1.20^{+0.78}_{-0.46}$	$0.59^{+0.54}_{-0.48}$	$0.96^{+0.82}_{-0.53}$
$z = 2$					
Ms Fs	All	$1.02^{+0.10}_{-0.09}$	$0.98^{+0.27}_{-0.18}$	$1.12^{+0.41}_{-0.33}$	$1.15^{+1.04}_{-0.96}$
	>0.14	$0.96^{+0.06}_{-0.06}$	$0.97^{+0.10}_{-0.12}$	$1.09^{+0.26}_{-0.26}$	$1.38^{+0.69}_{-0.99}$
	<0.14	$1.09^{+0.06}_{-0.13}$	$1.04^{+0.25}_{-0.36}$	$1.17^{+0.45}_{-0.89}$	$1.01^{+1.30}_{-0.96}$
Ms Fp	All	$0.96^{+0.19}_{-0.16}$	$0.94^{+0.35}_{-0.39}$	$1.09^{+0.45}_{-0.68}$	$1.30^{+1.56}_{-1.02}$
	>0.14	$0.92^{+0.08}_{-0.31}$	$0.85^{+0.18}_{-0.23}$	$1.14^{+0.62}_{-0.75}$	$1.62^{+1.45}_{-0.94}$
	<0.14	$1.04^{+0.20}_{-0.18}$	$1.11^{+0.33}_{-0.57}$	$1.07^{+0.31}_{-0.66}$	$1.19^{+1.53}_{-1.04}$
Ms Sp	All	$0.91^{+0.41}_{-0.29}$	$0.96^{+0.53}_{-0.50}$	$1.01^{+0.82}_{-0.46}$	$0.87^{+1.25}_{-0.80}$
	>0.14	$0.75^{+0.23}_{-0.27}$	$0.67^{+0.34}_{-0.45}$	$1.06^{+0.89}_{-0.48}$	$1.19^{+1.33}_{-0.55}$
	<0.14	$1.12^{+0.29}_{-0.31}$	$1.18^{+0.52}_{-0.39}$	$0.99^{+0.65}_{-0.48}$	$0.51^{+1.21}_{-0.51}$
NMp Fs	All	$1.03^{+0.08}_{-0.07}$	$1.14^{+0.17}_{-0.24}$	$0.92^{+0.51}_{-0.60}$	$0.55^{+1.16}_{-0.34}$
	>0.14	$1.01^{+0.09}_{-0.08}$	$1.13^{+0.13}_{-0.21}$	$0.58^{+0.86}_{-0.35}$	$0.56^{+1.13}_{-0.39}$
	<0.14	$1.04^{+0.07}_{-0.07}$	$1.15^{+0.19}_{-0.27}$	$1.02^{+0.38}_{-0.60}$	$0.53^{+1.22}_{-0.30}$
NMp Fp	All	$1.03^{+0.15}_{-0.15}$	$1.25^{+0.33}_{-0.25}$	$0.28^{+0.92}_{-0.19}$	$0.90^{+0.90}_{-0.54}$
	>0.14	$1.02^{+0.13}_{-0.13}$	$1.17^{+0.21}_{-0.21}$	$0.26^{+0.37}_{-0.16}$	$0.74^{+0.94}_{-0.40}$
	<0.14	$1.05^{+0.16}_{-0.17}$	$1.38^{+0.42}_{-0.34}$	$0.36^{+1.08}_{-0.29}$	$1.06^{+0.78}_{-0.68}$
NMp Sp	All	$1.11^{+0.34}_{-0.24}$	$1.41^{+0.54}_{-0.32}$	$0.22^{+0.74}_{-0.15}$	$0.79^{+0.90}_{-0.47}$
	>0.14	$1.11^{+0.28}_{-0.21}$	$1.34^{+0.43}_{-0.31}$	$0.19^{+0.52}_{-0.11}$	$0.66^{+0.99}_{-0.39}$
	<0.14	$1.10^{+0.39}_{-0.25}$	$1.48^{+0.62}_{-0.32}$	$0.27^{+0.94}_{-0.21}$	$0.90^{+0.79}_{-0.50}$
$z = 3$					
Ms Fs	All	$1.01^{+0.12}_{-0.14}$	$0.99^{+0.39}_{-0.26}$	$0.97^{+0.69}_{-0.50}$	$1.09^{+2.02}_{-1.00}$
	>0.14	$0.90^{+0.10}_{-0.10}$	$0.80^{+0.26}_{-0.08}$	$0.98^{+0.93}_{-0.41}$	$1.10^{+1.28}_{-0.84}$
	<0.14	$1.09^{+0.10}_{-0.07}$	$1.18^{+0.28}_{-0.38}$	$0.97^{+0.35}_{-0.59}$	$0.62^{+2.52}_{-0.57}$
Ms Fp	All	$1.01^{+0.16}_{-0.15}$	$1.06^{+0.45}_{-0.29}$	$0.83^{+1.05}_{-0.74}$	$1.47^{+2.30}_{-1.33}$
	>0.14	$0.97^{+0.13}_{-0.12}$	$0.99^{+0.19}_{-0.25}$	$0.65^{+1.59}_{-0.54}$	$1.32^{+2.28}_{-1.20}$
	<0.14	$1.06^{+0.19}_{-0.14}$	$1.17^{+0.54}_{-0.33}$	$0.93^{+0.66}_{-0.87}$	$1.82^{+1.94}_{-1.68}$
Ms Sp	All	$0.97^{+0.27}_{-0.21}$	$1.10^{+0.31}_{-0.35}$	$0.44^{+0.91}_{-0.41}$	$1.62^{+2.48}_{-1.30}$
	>0.14	$0.94^{+0.28}_{-0.17}$	$1.02^{+0.30}_{-0.24}$	$0.23^{+0.61}_{-0.20}$	$1.75^{+2.65}_{-0.58}$
	<0.14	$1.00^{+0.26}_{-0.24}$	$1.12^{+0.45}_{-0.72}$	$0.78^{+0.93}_{-0.74}$	$1.60^{+1.65}_{-1.56}$
NMp Fs	All	$1.02^{+0.16}_{-0.09}$	$1.10^{+0.35}_{-0.19}$	$0.71^{+0.76}_{-0.60}$	$0.60^{+1.27}_{-0.53}$
	>0.14	$0.98^{+0.10}_{-0.10}$	$1.03^{+0.31}_{-0.12}$	$0.66^{+0.74}_{-0.28}$	$0.51^{+0.71}_{-0.45}$
	<0.14	$1.11^{+0.15}_{-0.15}$	$1.19^{+0.87}_{-0.30}$	$0.78^{+0.71}_{-0.75}$	$0.81^{+1.50}_{-0.73}$
NMp Fp	All	$1.07^{+0.16}_{-0.17}$	$1.21^{+0.26}_{-0.22}$	$0.46^{+0.96}_{-0.39}$	$1.11^{+1.17}_{-0.82}$

Table A2
(Continued)

Instruments	$W_{6.2}$	$\alpha_{\rm Tot}$	$\alpha_{\rm Sb}$	$\alpha_{\rm AGN}$	$\alpha_{\rm H}$
	>0.14	$1.05^{+0.13}_{-0.14}$	$1.19^{+0.21}_{-0.17}$	$0.22^{+0.54}_{-0.15}$	$0.95^{+1.23}_{-0.83}$
	<0.14	$1.08^{+0.21}_{-0.21}$	$1.24^{+0.26}_{-0.33}$	$0.94^{+0.75}_{-0.81}$	$1.28^{+1.11}_{-0.89}$
NMp Sp	All	$1.11^{+0.28}_{-0.24}$	$1.30^{+0.39}_{-0.26}$	$0.29^{+1.27}_{-0.24}$	$1.14^{+1.29}_{-0.93}$
	>0.14	$1.15^{+0.23}_{-0.25}$	$1.28^{+0.33}_{-0.25}$	$0.21^{+0.80}_{-0.16}$	$1.05^{+1.73}_{-0.91}$
	<0.14	$1.08^{+0.34}_{-0.22}$	$1.32^{+0.49}_{-0.26}$	$0.63^{+1.47}_{-0.60}$	$1.23^{+0.99}_{-0.94}$
$z = 4$					
Ms Fs	All	$1.00^{+0.15}_{-0.28}$	$0.97^{+0.39}_{-0.49}$	$1.09^{+0.41}_{-0.54}$	$0.85^{+1.37}_{-0.80}$
	>0.14	$0.91^{+0.17}_{-0.19}$	$0.85^{+0.35}_{-0.31}$	$1.13^{+0.75}_{-0.57}$	$0.88^{+0.92}_{-0.78}$
	<0.14	$1.07^{+0.16}_{-0.15}$	$1.12^{+0.41}_{-0.64}$	$1.05^{+0.40}_{-0.77}$	$0.81^{+2.34}_{-0.77}$
Ms Fp	All	$1.00^{+0.21}_{-0.14}$	$1.07^{+0.37}_{-0.40}$	$0.51^{+0.84}_{-0.48}$	$2.10^{+2.08}_{-1.90}$
	>0.14	$0.98^{+0.15}_{-0.09}$	$0.99^{+0.41}_{-0.42}$	$0.33^{+1.85}_{-0.30}$	$2.16^{+1.03}_{-2.03}$
	<0.14	$1.01^{+0.25}_{-0.26}$	$1.12^{+0.36}_{-0.36}$	$0.73^{+0.55}_{-0.63}$	$2.07^{+2.80}_{-1.94}$
Ms Sp	All	$0.98^{+0.37}_{-0.29}$	$1.11^{+0.37}_{-0.49}$	$0.29^{+1.82}_{-0.26}$	$1.36^{+2.12}_{-1.11}$
	>0.14	$0.94^{+0.36}_{-0.24}$	$1.01^{+0.26}_{-0.46}$	$0.34^{+2.84}_{-0.32}$	$1.31^{+1.27}_{-0.91}$
	<0.14	$1.03^{+0.36}_{-0.35}$	$1.24^{+0.43}_{-0.53}$	$0.26^{+1.45}_{-0.20}$	$1.63^{+2.65}_{-1.47}$
NMp Fs	All	$0.98^{+0.13}_{-0.11}$	$1.04^{+0.25}_{-0.17}$	$0.91^{+0.36}_{-0.47}$	$0.69^{+0.94}_{-0.58}$
	>0.14	$0.92^{+0.16}_{-0.06}$	$0.95^{+0.22}_{-0.11}$	$0.92^{+0.35}_{-0.40}$	$0.48^{+1.36}_{-0.38}$
	<0.14	$1.04^{+0.11}_{-0.10}$	$1.12^{+0.31}_{-0.21}$	$0.90^{+0.32}_{-0.54}$	$0.89^{+0.57}_{-0.77}$
NMp Fp	All	$1.05^{+0.17}_{-0.16}$	$1.19^{+0.45}_{-0.24}$	$0.55^{+0.83}_{-0.44}$	$1.08^{+2.05}_{-0.73}$
	>0.14	$1.00^{+0.19}_{-0.12}$	$1.11^{+0.42}_{-0.18}$	$0.46^{+0.68}_{-0.40}$	$0.76^{+1.28}_{-0.41}$
	<0.14	$1.09^{+0.17}_{-0.17}$	$1.25^{+0.48}_{-0.27}$	$0.79^{+0.68}_{-0.62}$	$1.59^{+2.05}_{-1.25}$
NMp Sp	All	$1.12^{+0.64}_{-0.25}$	$1.24^{+0.33}_{-0.38}$	$0.47^{+4.68}_{-0.40}$	$1.45^{+1.98}_{-1.29}$
	>0.14	$1.13^{+0.48}_{-0.18}$	$1.21^{+0.25}_{-0.27}$	$0.43^{+5.74}_{-0.39}$	$1.19^{+2.02}_{-1.04}$
	<0.14	$1.11^{+0.87}_{-0.32}$	$1.29^{+0.35}_{-0.48}$	$0.55^{+4.19}_{-0.46}$	$1.64^{+1.94}_{-0.95}$
$z = 5$					
Ms Fs	All	$0.97^{+0.19}_{-0.25}$	$0.98^{+0.31}_{-0.55}$	$1.01^{+0.42}_{-0.91}$	$1.28^{+2.73}_{-0.62}$
	>0.14	$0.87^{+0.10}_{-0.34}$	$0.80^{+0.24}_{-0.43}$	$0.86^{+0.41}_{-0.71}$	$1.27^{+1.73}_{-0.63}$
	<0.14	$1.07^{+0.16}_{-0.12}$	$1.12^{+0.31}_{-0.41}$	$1.09^{+0.35}_{-1.04}$	$1.28^{+3.65}_{-0.33}$
Ms Fp	All	$1.05^{+0.23}_{-0.34}$	$1.04^{+0.47}_{-0.56}$	$0.73^{+1.21}_{-0.67}$	$2.39^{+2.56}_{-1.62}$
	>0.14	$1.04^{+0.31}_{-0.40}$	$1.04^{+0.39}_{-0.49}$	$0.48^{+1.46}_{-0.43}$	$2.08^{+2.36}_{-1.21}$
	<0.14	$1.06^{+0.19}_{-0.22}$	$1.06^{+0.51}_{-0.58}$	$0.91^{+1.03}_{-0.72}$	$2.73^{+2.96}_{-2.54}$
Ms Sp	All	$0.96^{+0.33}_{-0.35}$	$1.07^{+0.40}_{-0.78}$	$0.14^{+1.51}_{-0.12}$	$2.02^{+4.61}_{-1.51}$
	>0.14	$0.97^{+0.19}_{-0.33}$	$1.06^{+0.31}_{-0.51}$	$0.07^{+0.98}_{-0.05}$	$1.66^{+5.87}_{-1.13}$
	<0.14	$0.93^{+0.51}_{-0.34}$	$1.07^{+0.52}_{-0.78}$	$0.34^{+2.39}_{-0.33}$	$2.17^{+3.76}_{-1.67}$
NMp Fs	All	$0.96^{+0.19}_{-0.18}$	$1.00^{+0.32}_{-0.47}$	$1.01^{+0.47}_{-0.40}$	$0.54^{+1.81}_{-0.37}$
	>0.14	$0.91^{+0.11}_{-0.16}$	$0.95^{+0.13}_{-0.28}$	$0.93^{+0.50}_{-0.25}$	$0.32^{+0.96}_{-0.17}$
	<0.14	$1.02^{+0.21}_{-0.18}$	$1.04^{+0.44}_{-0.60}$	$1.02^{+0.55}_{-0.97}$	$0.87^{+2.66}_{-0.64}$
NMp Fp	All	$1.08^{+0.20}_{-0.14}$	$1.28^{+0.50}_{-0.36}$	$0.60^{+0.84}_{-0.56}$	$0.73^{+2.12}_{-0.63}$
	>0.14	$0.99^{+0.24}_{-0.16}$	$1.10^{+0.37}_{-0.22}$	$0.43^{+0.87}_{-0.33}$	$0.49^{+1.74}_{-0.39}$
	<0.14	$1.14^{+0.16}_{-0.12}$	$1.47^{+0.45}_{-0.44}$	$0.63^{+0.83}_{-0.62}$	$0.94^{+2.94}_{-0.80}$
NMp Sp	All	$1.11^{+0.65}_{-0.23}$	$1.30^{+0.49}_{-0.35}$	$0.36^{+1.62}_{-0.31}$	$0.92^{+1.94}_{-0.73}$
	>0.14	$1.21^{+1.16}_{-0.19}$	$1.27^{+0.40}_{-0.41}$	$0.54^{+10.26}_{-0.46}$	$0.52^{+1.98}_{-0.37}$
	<0.14	$1.00^{+0.38}_{-0.23}$	$1.30^{+0.80}_{-0.32}$	$0.21^{+1.06}_{-0.18}$	$1.34^{+2.12}_{-1.05}$

Note. Results are presented for $z \sim 0$, $z = 0.5$, $z = 1$, $z = 2$, $z = 3$, $z = 4$, and $z = 5$. For each redshift, results are presented for simulations using the entire input sample, and for high- and low-PAH 6.2 μm EW subsamples (Section 6.3).

ORCID iDs

Duncan Farrah https://orcid.org/0000-0003-1748-2010
Kiana Ejercito https://orcid.org/0009-0002-6970-5247
Andreas Efstathiou https://orcid.org/0000-0002-2612-4840
David Leisawitz https://orcid.org/0000-0003-1000-2547
Athena Engholm https://orcid.org/0000-0001-6970-7782
Irene Shivaei https://orcid.org/0000-0003-4702-7561
Matteo Bonato https://orcid.org/0000-0001-9139-2342
David L. Clements https://orcid.org/0000-0002-9548-5033
Sara Petty https://orcid.org/0000-0003-0624-3276
Lura. K. Pitchford https://orcid.org/0000-0002-5206-5880
Charalambia Varnava https://orcid.org/0009-0004-6200-0919
Jose Afonso https://orcid.org/0000-0002-9149-2973
Carlotta Gruppioni https://orcid.org/0000-0002-5836-4056
Evanthia Hatziminaoglou https://orcid.org/0000-0003-0917-9636
Andrew Hoffman https://orcid.org/0000-0002-8732-6980
Mark Lacy https://orcid.org/0000-0002-3032-1783
Brenda C. Matthews https://orcid.org/0000-0003-3017-9577
Conor Nixon https://orcid.org/0000-0001-9540-9121
Chris Pearson https://orcid.org/0000-0001-6139-649X
Berke Vow Ricketti https://orcid.org/0000-0001-9701-5660
Dimitra Rigopoulou https://orcid.org/0000-0001-6854-7545
Loren Robinson https://orcid.org/0000-0003-0796-362X
Locke D. Spencer https://orcid.org/0000-0002-9941-2077
Lingyu Wang https://orcid.org/0000-0002-6736-9158
David B. Sanders https://orcid.org/0000-0002-1233-9998
Gerard van Belle https://orcid.org/0000-0002-8552-158X

References

Bernard-Salas, J., Spoon, H. W. W., Charmandaris, V., et al. 2009, ApJS, 184, 230
Béthermin, M., Bolatto, A. D., Boulanger, F., et al. 2024, A&A, 692, A52
Béthermin, M., Wu, H.-Y., Lagache, G., et al. 2017, A&A, 607, A89
Bisigello, L., Gruppioni, C., Bolatto, A., et al. 2024, A&A, 689, A125
Blain, A. W., Smail, I., Ivison, R. J., Kneib, J. P., & Frayer, D. T. 2002, PhR, 369, 111
Bonato, M., Leisawitz, D., De Zotti, G., et al. 2024, ApJ, 977, 208
Boquien, M., Burgarella, D., Roehlly, Y., et al. 2019, A&A, 622, A103
Bradford, C. M. M., Kogut, A. J., Fixsen, D., et al. 2025, JATIS, 11, 031627
Burgarella, D., Ciesla, L., Sauvage, M., et al. 2024, SPIE, 13092, 130923B
Casey, C. M., Narayanan, D., & Cooray, A. 2014, PhR, 541, 45
Chevallard, J., & Charlot, S. 2016, MNRAS, 462, 1415
Chin, G., Anderson, C. M., Bergner, J., et al. 2024, JATIS, 10, 042310
Ciesla, L., Dowell, C. D., Sauvage, M., et al. 2025, JATIS, 11, 031625
Clements, D. L., Pearson, C., Farrah, D., et al. 2018, MNRAS, 475, 2097
Condon, J. J. 1974, ApJ, 188, 279
da Cunha, E., Charlot, S., & Elbaz, D. 2008, MNRAS, 388, 1595
de Graauw, T., Haser, L. N., Beintema, D. A., et al. 1996, A&A, 315, L49
Desai, V., Armus, L., Spoon, H. W. W., et al. 2007, ApJ, 669, 810
Donnellan, J. M. S., Oliver, S. J., Béthermin, M., et al. 2024, MNRAS, 532, 1966
Efstathiou, A., Christopher, N., Verma, A., & Siebenmorgen, R. 2013, MNRAS, 436, 1873
Efstathiou, A., Farrah, D., Afonso, J., et al. 2022, MNRAS, 512, 5183
Efstathiou, A., Hough, J. H., & Young, S. 1995, MNRAS, 277, 1134
Efstathiou, A., & Rowan-Robinson, M. 1995, MNRAS, 273, 649
Efstathiou, A., & Siebenmorgen, R. 2009, A&A, 502, 541
Egami, E., Gallerani, S., Schneider, R., et al. 2018, PASA, 35, e048
Elias, J. H., Joyce, R. R., Liang, M., et al. 2006, SPIE, 6269, 62694C
Farrah, D., Afonso, J., Efstathiou, A., et al. 2003, MNRAS, 343, 585
Farrah, D., Baloković, M., Stern, D., et al. 2016, ApJ, 831, 76
Farrah, D., Bernard-Salas, J., Spoon, H. W. W., et al. 2007, ApJ, 667, 149
Farrah, D., Efstathiou, A., Afonso, J., et al. 2022, MNRAS, 513, 4770
Farrah, D., Lebouteiller, V., Spoon, H. W. W., et al. 2013, ApJ, 776, 38
Farrah, D., Smith, K. E., Ardila, D., et al. 2019, JATIS, 5, 020901
Finkbeiner, D. P., Davis, M., & Schlegel, D. J. 1999, ApJ, 524, 867
Gao, F., Wang, L., Efstathiou, A., et al. 2021, A&A, 654, A117
Glenn, J., Meixner, M., Bradford, C. M., et al. 2025, JATIS, 11, 031628
Griffin, M. J., Abergel, A., Abreu, A., et al. 2010, A&A, 518, L3

Hatziminaoglou, E., Fritz, J., Franceschini, A., et al. 2008, MNRAS, 386, 1252
Hatziminaoglou, E., Fritz, J., & Jarrett, T. H. 2009, MNRAS, 399, 1206
Herrero-Illana, R., Pérez-Torres, M. Á., Randriamanakoto, Z., et al. 2017, MNRAS, 471, 1634
Hogg, D. W. 2001, AJ, 121, 1207
Holland, W. S., Bintley, D., Chapin, E. L., et al. 2013, MNRAS, 430, 2513
Houck, J. R., Roellig, T. L., van Cleve, J., et al. 2004, ApJS, 154, 18
Hunt, L. K., De Looze, I., Boquien, M., et al. 2019, A&A, 621, A51
Hurley, P. D., Oliver, S., Betancourt, M., et al. 2017, MNRAS, 464, 885
Jakobsen, P., Ferruit, P., Alves de Oliveira, C., et al. 2022, A&A, 661, A80
Kiss, C., Klaas, U., & Lemke, D. 2005, A&A, 430, 343
Kool, E. C., Reynolds, T. M., Mattila, S., et al. 2020, MNRAS, 498, 2167
Leinert, C., Ábrahám, P., Acosta-Pulido, J., Lemke, D., & Siebenmorgen, R. 2002, A&A, 393, 1073
Leisawitz, D., Baker, C., Barger, A., et al. 2007, AdSpR, 40, 689
Leja, J., Carnall, A. C., Johnson, B. D., Conroy, C., & Speagle, J. S. 2019, ApJ, 876, 3
Li, J. I. H., Shen, Y., Ho, L. C., et al. 2021, ApJ, 906, 103
Lin, Y.-W., Wu, C. K.-W., Ling, C.-T., et al. 2024, MNRAS, 527, 11882
Lonsdale, C. J., Farrah, D., & Smith, H. E. 2006, in Astrophysics Update 2, ed. J. W. Mason (Praxis Publishing), 285
Lonsdale, C. J., Lacy, M., Kimball, A. E., et al. 2015, ApJ, 813, 45
Lyu, J., & Rieke, G. H. 2022, ApJL, 940, L31
Magris, C. G., Mateu, P. J., Mateu, C., et al. 2015, PASP, 127, 16
Mather, J. C., Cheng, E. S., Cottingham, D. A., et al. 1994, ApJ, 420, 439
Mattila, S., Pérez-Torres, M., Efstathiou, A., et al. 2018, Sci, 361, 482
Mitchell, P. D., Lacey, C. G., Baugh, C. M., & Cole, S. 2013, MNRAS, 435, 87
Mroczkowski, T., Gallardo, P. A., Timpe, M., et al. 2025, A&A, 694, A142
Pacifici, C., Iyer, K. G., Mobasher, B., et al. 2023, ApJ, 944, 141
Papoular, R. 1983, A&A, 117, 46
Pearson, C., Rigopoulou, D., Hurley, P., et al. 2016, ApJS, 227, 9
Pearson, W. J., Wang, L., Hurley, P. D., et al. 2018, A&A, 615, A146
Pearson, W. J., Wang, L., van der Tak, F. F. S., et al. 2017, A&A, 603, A102
Pérez-Torres, M., Mattila, S., Alonso-Herrero, A., Aalto, S., & Efstathiou, A. 2021, A&ARv, 29, 2
Poglitsch, A., Waelkens, C., Geis, N., et al. 2010, A&A, 518, L2
Rayner, J. T., Toomey, D. W., Onaka, P. M., et al. 2003, PASP, 115, 362
Ricketti, B. V., Spencer, L. D., Leisawitz, D. T., et al. 2024, SPIE, 13095, 130951T
Rieke, M. J., Kelly, D. M., Misselt, K., et al. 2023, PASP, 135, 028001
Sanders, D. B., & Mirabel, I. F. 1996, ARA&A, 34, 749
Sommovigo, L., & Algera, H. 2025, MNRAS, 540, 3693
Sorba, R., & Sawicki, M. 2015, MNRAS, 452, 235
Spilker, J., Levy, R. C., Marrone, D. P., et al. 2024, JATIS, 10, 042305
Spinoglio, L., Fernández-Ontiveros, J. A., & Malkan, M. A. 2024, ApJ, 964, 117
Spoon, H. W. W., Farrah, D., Lebouteiller, V., et al. 2013, ApJ, 775, 127
Takagi, T., Ohyama, Y., Goto, T., et al. 2010, A&A, 514, A5
Takeuchi, T. T., & Ishii, T. T. 2004, ApJ, 604, 40
Thorne, J. E., Robotham, A. S. G., Bellstedt, S., & Davies, L. J. M. 2023, MNRAS, 522, 6354
Tokunaga, A. T., Kobayashi, N., Bell, J., et al. 1998, SPIE, 3354, 512
Varnava, C., & Efstathiou, A. 2024, MNRAS, 531, 2304
Varnava, C., Efstathiou, A., & Farrah, D. 2024, MNRAS, 534, 2585
Varnava, C., Efstathiou, A., Farrah, D., & Rigopoulou, D. 2025, MNRAS, 538, 426
Wang, L., La Marca, A., Gao, F., et al. 2024, A&A, 688, A20
Weaver, J. R., Zalesky, L., Kokorev, V., et al. 2023, ApJS, 269, 20
Wright, G. S., Rieke, G. H., Glasse, A., et al. 2023, PASP, 135, 048003
Yamada, S., Ueda, Y., Herrera-Endoqui, M., et al. 2023, ApJS, 265, 37